Cell-extrinsic autophagy in mature adipocytes regulates anti-inflammatory response to intestinal tissue injury through lipid mobilization

Felix Clemens Richter[1], Matthias Friedrich[1,2], Mathilde Pohin[1,*], Ghada Alsaleh[1,*], Irina Guschina[3], Sarah Karin Wideman[4], Errin Johnson[5], Mariana Borsa[1], Klara Piletic[1], Paula Hahn[1], Henk Simon Schipper[1,6], Claire M. Edwards[7,8], Fiona Powrie[1], Anna Katharina Simon[1,#]

*Authors contributed equally.

#Corresponding author: katja.simon@imm.ox.ac.uk

Affiliations

[1] Kennedy Institute of Rheumatology, Roosevelt Drive, OX3 7FY, Oxford, United Kingdom
[2] Translational Gastroenterology Unit, John Radcliffe Hospital, Nuffield Department of Medicine, University of Oxford, Headley Way, OX3 9DU, Oxford, United Kingdom
[3] School of Biosciences, Cardiff University, Cardiff CF10 3AX, United Kingdom
[4] MRC Human Immunology Unit, MRC Weatherall Institute of Molecular Medicine, University of Oxford, John Radcliffe Hospital, Oxford, United Kingdom
[5] The Dunn School of Pathology, South Parks Road, Oxford OX1 3RE, United Kingdom
[6] Center for Translational Immunology, University Medical Center Utrecht, The Netherlands
[7] Nuffield Department of Orthopaedics, Rheumatology and Musculoskeletal Sciences, Botnar Research Centre, OX3 7LD, Oxford, United Kingdom
[8] Nuffield Department of Surgical Sciences, Botnar Research Centre OX3 7LD, Oxford, United Kingdom

Summary

Autophagy is a critical cellular recycling pathway which is genetically linked to the development of intestinal inflammation in humans. Inflammation drives adipose tissue breakdown and provision of major nutrients such as free fatty acids (FFA). However, the effect of autophagy-mediated FFA release by adipocytes in immune-mediated inflammatory diseases remains unexplored.

In a mouse model of intestinal inflammation, we found that visceral adipocytes upregulate autophagy at peak inflammation. Adipocyte-specific loss of the key autophagy gene *Atg7* (*Atg7*^{Ad}) resulted in the exacerbation of intestinal inflammation. TNFα-induced lipolysis was impaired in *Atg7*-deficient adipocytes leading to the reduced availability of several FFA species, and decreased expression of the FFA transporter CD36 on adipose tissue macrophages (ATMs). Visceral adipose tissues from *Atg7*^{Ad} mice released less IL-10 resulting in lower levels of circulating IL-10 in colitis. ATMs present the main source of adipose tissue-derived IL-10 during colitis. *In vitro* assays confirmed that FFA restriction from macrophages reduced CD36 expression and diminished IL-10 production.

Taken together, our study demonstrates that autophagy-mediated FFA release from adipocytes directs anti-inflammatory responses in ATMs, which in turn conveys protective effects for distant intestinal inflammation.

Key words: Adipose Tissue, Macrophage, Autophagy, IBD, Colitis, Adipocyte, IL-10

Introduction

Autophagy is an essential cellular recycling pathway that engulfs cellular contents, including organelles and macromolecules, in a double membraned autophagosome and directs them towards lysosomal degradation. The released nutrients can then be used for both biosynthetic building blocks and energy generation (Riffelmacher et al., 2018). Immune cells are cell-intrinsically reliant on autophagy during their differentiation and for their immune functions (Clarke and Simon, 2019). For instance, neutrophils require autophagy for the liberation of free fatty acids (FFA) from their intracellular lipid droplet stores in order to generate energy through oxidative phosphorylation (Riffelmacher et al., 2017). Similarly, autophagy-deficient macrophages are arrested in a glycolytic metabolic program promoting expression of pro-inflammatory cytokines and reactive oxygen species (Kang et al., 2016; Stranks et al., 2015). While the cell-intrinsic need for recycled nutrients is evident, whether these mobilized nutrients can also be provided to immune cells in an autophagy-dependent manner remains less well understood. In plants, nutrients recycled via autophagy are mobilized to other plant organs or stored in seeds (Guiboileau et al., 2013; Guiboileau et al., 2012). In animals, only a few pioneering studies have looked at the mobilization of nutrients, in particular amino acids. For instance, autophagy in non-cancer cells control amino acid availability and thus tumour growth (Katheder et al., 2017; Poillet-Perez et al., 2018; Sousa et al., 2016). Activation of autophagy in hepatic stellate cells by the cancer cell induces the release and provision of alanine to the cancer cell (Sousa et al., 2016). Despite mounting evidence for autophagy-dependent amino acid mobilization, it remains unclear whether this also exists for other nutrients such as FFA.

Adipocytes are highly specialized cells responsible for the conversion and storage of energy-rich nutrients in form of lipids and for their release during times of high nutrient demand. In addition, the adipose tissue represents an important immunological organ harbouring a variety of immune cells, which are highly adapted to live in lipid-rich environments, such as macrophages (Grant and Dixit, 2015). Lean adipose tissues are predominantly populated by tissue-resident M2-type macrophages, while inflammation as induced by obesity, subverts their tissue homeostatic functions and promotes pro-inflammatory M1-type polarization (Russo and Lumeng, 2018). M2-type macrophages require the uptake of exogenous lipids through CD36 expression and subsequently increase fatty acid oxidation-based metabolism (Huang et al., 2014). To-date, little is known about the function and reaction of

adipose tissue macrophages (ATMs) to other inflammatory conditions in metabolically healthy animals. In the context of osteoarthritis, adipose tissues were recently shown to contribute to inflammation and disease progression (Collins et al., 2021). This demonstrates an existing inter-tissue crosstalk of adipose tissues with distal tissue sites in immune-mediated inflammation.

Inflammatory bowel diseases (IBD) including its two predominant forms, Crohn's disease (CD) and ulcerative colitis (UC), describe a complex spectrum of intestinal inflammation. Epidemiological studies linked mutations in autophagy-related genes to an increased susceptibility for the development of IBD, in particular CD (Hampe et al., 2007; Jostins et al., 2012; McCarroll et al., 2008). Mechanistic studies showed that ablation of autophagy in immune and epithelial cells promotes intestinal inflammation (Cadwell et al., 2008; Cadwell et al., 2009; Kabat et al., 2016). In addition to the strong genetic association of autophagy and IBD, CD patients often present with an expansion of the mesenteric adipose tissue around the inflamed intestine, indicating an active involvement of the adipose tissue in the disease pathology (Sheehan et al., 1992).

Here, we sought to investigate the cell-extrinsic impact of adipocyte autophagy on the immune system during inflammation of a distant organ, the large intestine. We observed that autophagy is induced in mature adipocytes upon intestinal tissue injury, and that loss of autophagy, specifically in adipocytes, exacerbates the intestinal inflammation response to dextran sulphate sodium (DSS). Mechanistically, autophagy in mature adipocytes is required for the optimal release of FFA during inflammation. Local FFA restriction results in a limited production of IL-10 from ATMs, aggravating intestinal inflammation. Taken together, we demonstrate for the first time that adipocytes employ autophagy for lipid mobilization to promote the anti-inflammatory function of ATMs in order to control immune exacerbation at a distant organ.

Materials and Methods

Mice

Adipoq-CreERT2 mice (Sassmann et al., 2010) were purchased from Charles River, UK (JAX stock number: 025124) and were crossed to *Atg7* floxed mice (Komatsu et al., 2005). Experimental cages were sex- and age-matched and balanced for genotypes. Genetic recombination was induced at 8-10 weeks of age by oral gavage of 4mg tamoxifen per mouse for five consecutive days. All experimental procedures were conducted two weeks after last tamoxifen administration (Figure 2A). Wild-type C57BL/6J mice were purchased from Charles River, UK (JAX stock number: 0000664) or bred in-house. Mice were housed on a 12-hour dark/light cycle and fed *ad libitum*, under specific pathogen-free conditions. All animal experimentation was performed in accordance to approved procedures by the Local Review Committee and the Home Office under the project licence (PPL30/3388 and P01275425).

Murine models of intestinal inflammation

DSS-induced colitis was induced by 1.5-2% (w/v) DSS (MP Biomedicals, 160110) in drinking water. Mice were treated with DSS for five days and assessed at day 7, a peak inflammation time (Figure 1A), or at day 14, a resolution time point (Figure S3A). For *Helicobacter hepaticus* anti-IL10 receptor-induced colitis (Danne et al., 2017), mice were injected with 50mg/kg anti-IL-10 receptor antibody (clone 1B1.2, 2BScientific) intraperitoneally on day 0 and day 7 of the experiment. *H. hepaticus* was orally administered ($1x10^8$ colony forming units per mouse) by gavage for two consecutive days at day 0 and 1 of the experiment (Figure S4A). Uninfected control animals were kept in separate cages on the same rack. During intestinal inflammation experiments, we grouped water-treated $Atg7^{\Delta d}$ and wild-type littermate controls combined to visualize baseline levels.

Histopathology assessment

Distal, mid and proximal colon pieces were fixed in 10% neutral buffered formalin for 24 hours before washed and transferred into 70% ethanol. Tissue pieces from each sample were embedded in the same paraffin block and 5μm sections were subsequently stained with haematoxylin and eosin (H&E). Scoring of histology sections was executed in a blinded fashion according to a previously reported scoring system (Dieleman et al., 1998). In brief, each section was assessed for the degree inflammation, the

depth of tissue damage, possible crypt damages, with high scores signifying increased tissue damage. In addition, signs of regeneration were assessed, with high scores indicating delayed regeneration. Changes were multiplied with a factor classifying the involvement tissue area.

Adipose tissue and colon digestion

We collected mesenteric adipose tissue separate from a collective set of visceral adipose tissue depots (including omental, gonadal and retroperitoneal adipose tissue) to distinguish proximal versus distal effects of intestinal inflammation on adipose tissues. Adipose tissues were collected and digested in DMEM containing 1% fatty acid-free BSA (Sigma, 126609), 5% HEPES (Gibco, 15630-056), 0.2mg/mL Liberase TL (Roche, 5401020001) and 20μg/mL DNaseI (Roche, 11284932001). Tissues were minced in digestion medium and incubated for 25-30min at 37°C at 180rpm. Tissues were further broken down by pipetting using wide-bore tips and filtered through a 70μm mesh. Digestion was quenched by adding medium containing 2mM EDTA. Adipocyte and stromal vascular fraction were separated by centrifugation (700g, 10min) and collected for further downstream analysis.

Colon digestions were performed as previously described (Danne et al., 2017). Colons were opened longitudinally and faecal content was removed by washing with PBS. Then colons were washed twice in RPMI containing 5% FBS and 5mM EDTA at 37°C under agitation. Tissues were minced and digested in RPMI supplemented with 5% FBS, 1mg/mL collagenase type VIII (Sigma) and 40µg/mL DNaseI (Roche). Cell suspension was strained through 40μm mesh and cells were subjected to downstream analysis.

Flow Cytometry

Flow cytometry staining was performed as previously described (Riffelmacher et al., 2017). Surface staining was performed by incubating cells with fluorochrome-conjugated antibodies (Biolegend, BD Bioscience, eBioscience) and LIVE/DEAD Fixable Stains (ThermoFischer) for 20min at 4°C. Cells were fixed with 4% PFA for 10min at room temperature. For intracellular staining of transcription factors, cells were fixed/permeabilized using the eBioscience™ Foxp3/ Transcription Factor Staining Set (00-5523-00, Invitrogen). For cytokine staining, cells were stimulated using Cell Activation cocktail (Biolegend) for 4h at 37°C in RPMI containing 10% FBS. After surface staining, cells were fixed and stained in

Cytofix/CytoPerm (BD Bioscience) following manufacturer protocol. Samples were acquired on LSRII or Fortessa X-20 flow cytometers (BD Biosciences).

Quantitative PCR

Adipocytes and adipose tissue RNA were extracted using TRI reagent (T9424, Sigma). Colon tissue RNA were extracted in RLT buffer containing 1,4-Dithiothreitol. Tissues were homogenised by lysis in 2mL tubes containing ceramic beads (KT03961-1-003.2, Bertin Instruments) using a Precellys 24 homogenizer (Bertin Instruments). RNA was purified following RNeasy Mini Kit (74104, Qiagen) manufacturer instructions. cDNA was synthesized following the High-Capacity RNA-to-cDNA™ kit protocol (4388950, ThermoFischer). Gene expression was assessed using validated TaqMan probes and run on a ViiA7 real-time PCR system. All data were collected by comparative Ct method either represented as relative expression ($2^{-\Delta Ct}$) or fold change ($2^{-\Delta\Delta Ct}$). Data were normalized to the two most stable housekeeping genes; for adipose tissues *Tbp* and *Rn18s* and for colon *Actb* and *Hprt*.

Bulk RNA sequencing

Visceral adipocytes were isolated as floating fraction upon digestion. RNA was extracted and converted to cDNA as described above. PolyA libraries were prepared through end reparation, A-tailing and adapter ligation. Samples were then size-selected, multiplexed and sequenced using a NovaSeq6000. Raw read quality control was performed using pipeline readqc.py (https://github.com/cgat-developers/cgat-flow). Resulting reads were aligned to GRCm38/Mm10 reference genome using the pseudoalignment method kallisto (Bray et al., 2016). Differential gene expression analysis was performed using DEseq2 v1.30.1 (Love et al., 2014). Pathway enrichment analysis was performed on differentially expressed genes for “Biological Pathways” using clusterProfiler (v4.0) R package (Wu et al., 2021). Heatmaps of selected gene sets were presented as z-scores using R package pheatmap. R code is available under https://github.com/cleete/IBD-Adipocyte-Autophagy

Shotgun lipidomics

Serum lipidomics were performed using Shotgun Lipidomics platform by LipoType GmbH (Dresden, Germany), as described previously (Surma et al., 2015). In brief, serum lipids were isolated using methyl

tert-butyl ether and methanol extraction and lipid class specific internal standards were added. Extracts were analysed by mass spectrometry on a hybrid quadrupole/Orbitrap mass spectrometer. Lipid identification was performed through LipotypeXplorer software. Data was stratified according to mass accuracy, occupation threshold, noise, background and then normalized. Lipid standards were used for quantification. Values were returned when falling into lipid standard and coefficient variation for each lipid class. Lipids with missing values (due to failed GC or subthreshold) were removed from analysis. Dataset was analysed in R and code is available under: https://github.com/cleete/IBD-Adipocyte-Autophagy

Lipolysis assays

Adipose tissues were collected and washed in PBS before subjected to lipolysis assays. For isoproterenol stimulation, adipose tissues were cut into small tissue pieces and incubated in serum-free DMEM - High Glucose (Sigma, D5796) with 2% fatty acid-free BSA (Sigma, 126579) in the absence or presence of 10μM isoproterenol (Sigma, I6504) for the indicated time. TNFα-induced lipolysis was induced as previously described (Ju et al., 2019). In brief, small adipose tissue pieces were cultured in DMEM – High Glucose for 24 hours in the absence or presence of 100ng/mL recombinant TNFα (Peprotech, 315-01A) and then transferred into serum-free DMEM containing 2% fatty acid free BSA for 3 hours. Supernatants were collected and FFA concentration normalized to adipose tissue input.

Free fatty acid analysis

Total supernatant and serum FFA levels were measured using Free Fatty Acid Assay Quantification Kit (ab65341, Abcam). For detailed analysis of FFA species, lipids were extracted by Folch's method (Folch et al., 1957) and subsequently run on a one-dimensional thin layer chromatography (TLC) using a 10x10cm silica gel G plate in a hexane/diethyl ether/acetic acid (80:20:1, by vol.) solvent system. Separated FFA were used for fatty acid methyl esters (FAMEs) preparation through addition of 2.5% H_2SO_4 solution in dry methanol/toluene (2:1 (v/v)) at 70°C for 2h. A known amount of C17:0 was added as an internal standard for quantification. FAMEs were extracted with HPLC grade hexane. A Clarus 500 gas chromatograph with a flame ionizing detector (FID) (Perkin-Elmer) and fitted with a 30m x 0.25mm i.d. capillary column (Elite 225, Perkin Elmer) was used for separation and analysis of FAs.

The oven temperature was programmed as follows: 170°C for 3min, increased to 220°C at 4°C/min), and then held at 220°C for 15min. FAMEs were identified routinely by comparing retention times of peaks with those of G411 FA standards (Nu-Chek Prep Inc). TotalChrom software (Perkin-Elmer) was used for data acquisition and quantification.

Immunoblotting

Autophagic flux in adipose tissues was measured by incubating adipose tissue explants from experimental animals in RPMI in the absence or presence of lysosomal inhibitors 100nM Bafilomycin A1 and 20mM NH_4Cl for 4 hours. DMSO was used as 'vehicle' control. Adipose tissues were collected and snap frozen. Protein extraction was performed as previously described (An and Scherer, 2020). In brief, 500μL of lysis buffer containing protease inhibitors (04693159001, Roche) and phosphoStop (04906837001, Roche) were added per 100mg of tissue. Cells were lysed using Qiagen TissueLyser II. Tissues were incubated on ice for 1h and lipid contamination was removed via serial centrifugation and transfer of internatant into fresh tubes. Protein concentration was determined by BCA Protein Assay Kit (23227, Thermo Scientific). Total of 15-30μg protein were separated on a 4-12% Bis-Tris SDS PAGE and transferred using BioRad Turbo Blot (1704156, BioRad) onto PVDF membrane. Membranes were blocked in TBST containing 5% milk. Primary antibodies were used at indicated concentration overnight. Membranes were visualized using IRDye secondary antibodies (LICOR). Band quantification of Western Blots was performed on ImageJ. Autophagic flux was calculated as: (LC3-II (Inh) – LC3-II (Veh))/(LC3-II (Veh)), as previously described (Zhang et al., 2019).

Transmission electron microscopy

Mice were sacrificed by increasing concentrations of CO_2. Adipose tissues were excised, cut into small 1-2mm pieces and immediately fixed in pre-warmed (37 ˚C) primary fixative containing 2.5% glutaraldehyde and 4% formaldehyde in 0.1M sodium cacodylate buffer, pH7.2 for 2 hours at room temperature and then stored in the fixative at 4 ˚C until further processing. Samples were then washed for 2x 45 min in 0.1M sodium cacodylate buffer (pH 7.2) at room temperature with rotation, transferred to carrier baskets and processed for EM using a Leica AMW automated microwave processing unit. Briefly, this included three washes with 0.1M sodium cacodylate buffer, pH 7.2, one wash with 50mM

glycine in 0.1M sodium cacodylate buffer to quench free aldehydes, secondary fixation with 1% osmium tetroxide + 1.5% potassium ferricyanide in 0.1M sodium cacodylate buffer, six water washes, tertiary fixation with 2% uranyl acetate, two water washes, then dehydration with ethanol from 30%, 50%, 70%, 90%, 95% to 100% (repeated twice). All of these steps were performed at 37 ˚C and 15-20W for 1-2 mins each, with the exception of the osmium and uranyl acetate steps, which were for 12 min and 9 min respectively. Samples were infiltrated with TAAB Hard Plus epoxy resin to 100% resin in the AMW and then processed manually at room temperature for the remaining steps. Samples were transferred to 2ml tubes filled with fresh resin, centrifuged for ~2mins at 2000g (to help improve resin infiltration), then incubated at room temperature overnight with rotation. The following day, the resin was removed and replaced with fresh resin, then the samples were centrifuged as above and incubated at room temperature with rotation for ~3 hrs. This step was repeated and then tissue pieces were transferred to individual Beem capsules filled with fresh resin and polymerised for 48 hrs at 60 ˚C. Once polymerised, blocks were sectioned using a Diatome diamond knife on a Leica UC7 Ultramicrotome. Ultrathin (90nm) sections were transferred onto 200 mesh copper grids and then post-stained with lead citrate for 5 mins, washed and air dried. Grids were imaged with a Thermo Fisher Tecnai 12 TEM (operated at 120 kV) using a Gatan OneView camera.

Extracellular cytokine measurements

Serum samples were collected by cardiac puncture and collected in Microtainer tubes (365978, BD Bioscience). Samples were centrifuged for 90sec at 15,000g and serum aliquots were snap-frozen until further analysis. Global inflammatory cytokine analysis of supernatants of adipose tissue explant cultures and serum were performed using LEGENDPlex™ Mouse Inflammation Panel (740446, Biolegend). TNFα and IL-10 levels were measured by TNFα Mouse Uncoated ELISA Kit (88-7324-86, Invitrogen) and IL-10 Mouse Uncoated ELISA Kit (88-7105-86, Invitrogen), respectively.

Bone marrow macrophage culture

Bone marrow macrophages were differentiated as previously described (Fischer et al., 2021). In brief, BM were flushed and differentiated over 7 days in RPMI supplemented with 100ng/mL M-CSF (315-02, Peprotech). Cells were seeded at day 7 and polarized for 16 hours the following day using: 100ng/mL

M-CSF, 100ng/mL IFNγ (315-05, Peprotech), 100ng/mL LPS (L8274, Sigma). Supernatant and cells were collected for subsequent flow cytometry and/or ELISA analysis.

Statistical Analysis

Data were tested for normality before applying parametric or non-parametric testing. For two groups unpaired Student's test or Mann-Whitney test were applied. Comparisons across more than two experimental groups were performed using One-Way or Two-Way ANOVA with Šídák multiple testing correction. Data were considered statistically significant when $p<0.05$ (*$p<0.05$, **$p<0.01$, ***$p<0.001$, ****$p<0.0001$). Typically, data were pooled from at least two experiments, if not otherwise indicated, and presented as mean ± SEM. Serum lipidomics were analysed based on a linear regression model and subsequent multiple t-testing. Data was visualized and statistics calculated in either GraphPad Prism 9 or R software.

Results

DSS-induced intestinal inflammation promotes autophagy in adipose tissues

To investigate whether autophagy in mature adipocytes is altered in response to intestinal inflammation, we deployed a mouse model of intestinal inflammation evoked by the administration of 1.5-2% DSS in drinking water (Figure 1A). As expected, treatment with DSS damaged the colonic epithelial architecture and triggered intestinal inflammation, as measured by body weight loss (Figure 1B), increased histopathological inflammation score (Figure S1A), shortened colon length (Figure S1B) and enlarged mesenteric lymph nodes (Figure S1C). In addition, DSS treatment resulted in a significantly higher infiltration of immune cells in the inflamed colon, which appeared to be predominantly of myeloid origin (Figure S1D-E). Next, we assessed the impact of DSS-induced colitis on the adipose tissue. In line with body weight loss, visceral adipose tissue mass was reduced (Figure 1C), as were serum FFA levels seven days after initial DSS administration (Figure 1D).

To assess changes in autophagy levels, adipose tissue explants from water- or DSS-treated animals were cultured in the absence or presence of lysosomal inhibitors and the accumulation of the lipidated autophagosomal marker LC3 protein (LC3-II) was quantified. DSS-induced intestinal inflammation substantially increased autophagic flux in mesenteric and in gonadal white adipose tissue (mWAT and gWAT, respectively) (Figure 1E), indicating that both adipose tissues proximal and distal to the intestine are responsive to the inflammation. Although this data suggests that autophagy in the adipose tissue is induced during colitis, several cell types, including adipose tissue immune cells, could be responsible for this change. To validate that adipocytes contribute to the increased autophagic flux in the adipose tissue, we first prepared adipose tissue for transmission electron microscopy. Autophagosomal double membrane structures were identified in adipocytes, predominantly from DSS-treated mice (Figure 1F). Additionally, we digested the adipose tissues and enriched for a floating adipocyte fraction and a pelleted stromal vascular fraction (SVF). Adipocyte fractions showed increased transcript levels of several *Atg8* homologues in DSS colitis, further demonstrating an increase in autophagic flux in this cell type (Figure 1G). In contrast, SVF containing adipose tissue-resident immune cells showed no transcriptional changes in *Atg8* expression (Figure 1G). Overall, these results indicate that autophagy is induced in adipocytes in response to DSS-induced colitis.

Loss of adipocyte autophagy does neither alter systemic nor intestinal immune homeostasis

Next, we addressed whether loss of autophagy in adipocytes affects immune development and intestinal inflammation at steady state. Given the crucial role of adipocyte autophagy during adipogenesis (Singh et al., 2009; Zhang et al., 2009) and to ensure normal adipocyte tissue formation, we established a tamoxifen-inducible knockout mouse model to ablate the essential autophagy gene *Atg7* specifically in mature adipocytes (*Atg7*^{Ad}) (Figure 2A). We first confirmed efficient deletion of *Atg7* and disruption of autophagic flux. Activation of Cre nuclear translocation by tamoxifen administration led to the significant reduction of *Atg7* transcript levels in visceral adipocytes (Figure 2B). This deletion was further confirmed on the protein level (Figure 2C). Importantly, the adipocyte-specific loss of ATG7 resulted in the interruption of conversion of LC3-I to LC3-II in the adipose tissue (Figure 2C), thus confirming effective disruption of the autophagic process in the adipose tissue.

Over the two-week time period, body weight development as well as adipose tissue mass remained unchanged between *Atg7*^{Ad} and littermate controls (Figure S2A-B). In line with this, adipocyte autophagy loss under homeostatic conditions did not alter immune cell frequencies in the gut-associated mesenteric and in a collection of gut-distal visceral adipose tissues (Figure S2D). Further characterization of immune cells in mesenteric and visceral adipose tissues (Figure S2C,F) showed that loss of adipocyte autophagy did not significantly alter neither myeloid (Figure S2E) nor lymphoid compartments (Figure S2G). CD206-expressing macrophages were still found as the predominant myeloid cell subset (Figure S2E) and frequencies of B and T lymphocytes (Figure S2G) and specific T cell populations remained unaltered after loss of adipocyte ATG7 (Figure S2H). Overall, the data suggest that adipocyte autophagy does not change the immune cell populations found in the adipose tissue of unchallenged mice.

Since several autophagy related genes have been associated with the development of spontaneous colitis (Cadwell et al., 2009), we further investigated whether adipocyte autophagy loss would influence intestinal morphology and immune cell composition. Morphologically, colons from wild-type and *Atg7*^{Ad} mice were comparable in length, and histopathological analysis did not reveal any contribution of adipocyte autophagy loss to inflammation (Figure 2D-E). In addition, total colonic immune cells frequencies and numbers remained unaltered (Figure 2F). Detailed immune cell profiling and histopathology did not reveal any impact of adipocyte autophagy loss on intestinal immune homeostasis

(Figure 2G-H). Taken together, adipocyte autophagy loss does not lead to the development of spontaneous colitis and immune cell populations in the intestine remained unaffected.

Loss of adipocyte autophagy exacerbates barrier damage-induced intestinal inflammation

Given that adipocyte autophagy is upregulated during DSS-induced intestinal inflammation, we next sought to determine the effects of autophagy loss in adipocytes during colitis. Since we were unable to find differences at homeostasis between the genotypes, we grouped both wild type and *Atg7*^{Ad} tamoxifen-treated homeostatic mice an untreated control group. Upon DSS-treatment (Figure 3A), *Atg7*^{Ad} mice showed increased body weight loss in comparison to littermate controls (Figure 3B). In addition, adipocyte autophagy-deficient mice treated with DSS showed a significant shortening of the colon when compared to their wild-type littermates during acute inflammation (Figure 3C). Blinded histopathological assessment confirmed that DSS-treated *Atg7*^{Ad} mice exhibited more severe tissue damage in all parts of the colon, significantly increased inflammation, and delayed regeneration (Figure 3D). Furthermore, we found increased gene expression of alarmins such as *Il1a* and *Il33*, pro-inflammatory cytokines *Tnfa*, *Ptx3*, *Ifng* and *Cxcl9* in *Atg7*^{Ad} mice (Figure 3E). Although total CD45^{+} immune cells numbers were comparable between adipocyte autophagy-deficient mice and littermate controls (Figure 3F), DSS-inflamed *Atg7*^{Ad} mice showed an increased frequency of monocytes infiltrating the intestinal tissue (Figure 3G). In particular, the number of MHCII-expressing, inflammatory monocytes were increased in the lamina propria of *Atg7*^{Ad} mice (Figure 3H). Taken together, these data demonstrate that loss of adipocyte autophagy exacerbates intestinal inflammation in the acute phase of DSS-induced colitis.

Intestinal inflammation induced by DSS is self-resolving (Ho et al., 2021). Therefore, we assessed the impact of adipocyte autophagy loss two weeks after DSS induction (Figure S3A). At this timepoint, we were unable to find any differences in colon length between *Atg7*^{Ad} and littermate controls and equally there were no significant histopathological differences observed between the groups (Figure S3B-C). While induction of colitis is lymphocyte-independent, it has been suggested that its resolution is also controlled by lymphocytes (Wang et al., 2015). Interestingly, frequencies and total numbers of colonic FOXP3^{+} regulatory T cells (Tregs) were decreased in adipocyte autophagy-deficient animals compared to wild-type animals (Figure S3D), despite not affecting disease recovery. Intestinal FOXP3^{+} Tregs are

368 classified into three distinct subsets based on co-expression of TH_2 and TH_{17} transcription factors
369 GATA3$^+$ and RORgt$^+$, respectively (Whibley et al., 2019). While all populations tended to be diminished
370 in *Atg7^{Ad}* mice, only RORgt$^-$ FOXP3$^+$ Tregs were significantly reduced (Figure S3E). This suggests that
371 adipocyte autophagy does not interfere with the resolution of intestinal inflammation.
372 To further delineate the impact of adipocyte autophagy on intestinal inflammation, we next assessed its
373 impact in another model of colitis. To this end, mice were treated with the pathobiont *Helicobacter*
374 *hepaticus (Hh)* by oral gavage and co-administration of IL-10 receptor blocking antibody allowed for
375 breakage of intestinal immune tolerance to *Hh (Danne et al., 2017)*. We measured the effects of
376 adipocyte autophagy loss at both peak inflammation and resolution stages, at 2 and 6 weeks post-*Hh*
377 infection, respectively (Figure S4A). Deletion of adipocyte autophagy did not affect colon histopathology
378 in *Hh*-induced animals at either time point (Figure S4B). Similarly, intestinal immune cell composition
379 at peak inflammation (Figure S4C-E) and resolution (Figure S4-F-H) was comparable between the
380 inflamed groups. Taken together, these data suggested that adipocyte autophagy loss exacerbates
381 intestinal inflammation in a colitis model induced by intestinal epithelial damage but not in a model of
382 tolerance breakdown in which IL-10 signalling is disrupted.
383
384 *Intestinal inflammation promotes autophagic and fatty acid metabolic transcriptional programs in*
385 *primary adipocytes*
386 At this point, it remained unclear how the loss of adipocyte autophagy mediates the increase in intestinal
387 inflammation during DSS-induced colitis. Previous studies identified that adipose tissues from inflamed
388 animals shift their transcriptional profile and exhibit increased expression of genes involved in
389 inflammatory pathways and cytokine production (Mustain et al., 2013). For example, adipocytes
390 produce pro-inflammatory cytokines such as IL-6 and TNFα upon inflammation (Hotamisligil, 2017). We
391 therefore hypothesized that autophagy may impact the transcriptional inflammatory profile of visceral
392 adipocytes during intestinal inflammation, thus promoting inflammation. In order to analyse autophagy-
393 dependent differences in adipocyte transcription profiles, visceral adipocytes were collected from mice
394 treated with DSS or water and subsequently sequenced. Since we anticipated sex-specific differences
395 in adipocyte transcription profiles (Oliva et al., 2020), we included the same number of male and female
396 mice in each experimental group (Figure 4A). As expected, sex-specific transcriptional changes

explained ~33% of the dataset variance (Figure 4B), in line with previous reports. While the treatment clearly separated the experimental groups in the principal component analysis (PCA), there was no major impact of the genotype on the transcriptomic dataset (Figure 4B). Reassuringly, visceral adipocytes from *Atg7*^{Ad} mice had a strong reduction in *Atg7* levels and an increase in estrogen receptor 1 (*Esr1*) expression, due to the Cre transgene expression (Figure S5A-B), when compared by differential gene expression analysis. In line with the PCA analysis, across the treatment groups only 17 genes were significantly upregulated and 15 genes were downregulated in *Atg7*-deficient visceral adipocytes compared to wild-type (Figure S5A-B). The limited effect of autophagy loss has previously been observed in other contexts (Cadwell et al., 2008). Importantly, this data suggests that the loss of adipocyte autophagy does not alter the transcriptional regulation of inflammatory pathways in the adipocytes themselves, neither during homeostasis nor DSS treatment.

Having confirmed that autophagy loss does not substantially affect the transcriptional profile of adipocytes in either homeostasis or DSS-induced colitis, we next compared non-inflamed to inflamed adipocytes from wild-type animals. More than 4700 genes were differentially regulated between these states (Figure S5C), among which 2415 were significantly upregulated and 2333 downregulated. Gene ontology analysis using *clusterProfiler* further revealed an enrichment in several gene sets (Figure 4C). Confirming our earlier results that adipocyte autophagy is affected by DSS-induced colitis (Figure 1G), intestinal inflammation led to an enrichment of genes involved in macroautophagy in visceral adipocytes (Figure 4D), in particular by an increased expression of several *Atg8* homologues (*Gabarap*, *Gabarapl1*, *Map1lc3a*, *Map1lc3b*) (Figure S5D). In addition, genes related to fatty acid metabolism were enriched in visceral adipocytes during intestinal inflammation (Figure 4E). Interestingly, genes encoding for key proteins involved in the lipolytic pathway such *Adrb3*, *Pnpla2*, *Lipe* and *Fabp4* were upregulated upon intestinal inflammation (Figure 4F), implicating a change in the lipolytic status of the adipocytes. The increase of lipolytic genes (*Lipe*, *Pnpla2*) and simultaneous decrease of lipogenic genes (*Dgat2*, *Lpl*) is similarly observed in cachexic conditions (Baazim et al., 2021). Overall, intestinal inflammation leads to a broad transcriptional response in visceral adipocytes, altering autophagy and fatty acid metabolism, among others. However, disruption of autophagy had only limited effects on the visceral adipocyte transcriptome, suggesting that autophagy may affect adipocytes on a post-transcriptional level.

Autophagy-deficient adipocytes differentially secrete fatty acids in response to TNFα

Our transcriptomic analysis suggested enhanced autophagic and lipolytic pathways in adipocytes upon colitis. Recent reports implicated autophagy in mature adipocytes in the secretion of FFA in response to β-adrenergic receptor-mediated lipolysis (Cai et al., 2018; Son et al., 2020). To confirm the importance of adipocyte autophagy for optimal lipolytic output, supernatant FFA levels were measured upon exposure of autophagy-deficient and –sufficient adipocyte tissues to isoproterenol. Strikingly, FFA secretion was reduced upon lipolysis stimulation in autophagy-deficient adipocytes (Figure S6A). TNFα, a crucial cytokine for human and murine IBD pathologies (Friedrich et al., 2019), can affect adipose tissue through inhibition of lipogenesis and by promoting FFA secretion (Cawthorn and Sethi, 2008). Furthermore, TNFα has also been implicated as a necessary component to elicit anti-inflammatory pathways during intestinal inflammation (Kojouharoff et al., 1997; Noti et al., 2010). Since we found transcriptional changes in both fatty acid metabolism and TNFα regulatory pathways in inflamed adipocytes (Figure 4C), we further investigated the effects of TNFα on adipocyte lipid metabolism in this context. Expression of the gene encoding for TNF receptor 1, *Tnfrsf1a*, was upregulated during DSS-induced inflammation in both genotypes, suggesting that TNFα-sensing was unaffected by the loss of adipocyte autophagy (Figure 5A). As expected, DSS-induced colitis leads to an up-regulation of circulating levels of TNFα (Figure 5B). Furthermore, TNFα is a potent inducer of adipocyte lipolysis (Green et al., 1994; Ryden et al., 2002), therefore we used adipose tissue explants from *Atg7*^{Ad} mice or littermate controls and stimulated them with recombinant TNFα. In the presence of TNFα, adipocytes turn on FFA secretion, however strikingly, autophagy-deficient adipocytes showed a significant reduction in FFA secretion upon TNFα stimulation (Figure 5C). Consistent with the decreased lipolytic activity of autophagy-deficient adipocytes, *Atg7*^{Ad} mice exhibit reduced serum FFA levels compared to wild-type littermates upon DSS colitis (Figure 5D). While autophagy is well-known to be a potential source of FFA, it remains unclear whether autophagy can affect specific FFA species more than others. To investigate this, serum samples from water and DSS-treated animals were analysed by GC-FID. Interestingly, the proportion of individual serum FFAs was unaffected by the loss of adipocyte autophagy (Figure 5E). However, confirming our initial findings, the serum concentration of several FFA species was reduced upon adipocyte autophagy loss, indicating that adipocyte autophagy controls overall FFA levels rather than specific FFAs (Figure 5F). The expression of cytosolic lipases in visceral

adipocytes remained comparable between DSS-treated wild-type and *Atg7*^{Ad} mice, suggesting that autophagy regulates FFA secretion on a post-transcriptional level (Figure S6B).

In addition to controlling circulating FFA levels, adipocytes take part in the control of other serum lipid species. Therefore, using an unbiased approach, the serum lipidome of *Atg7*^{Ad} and wild-type littermate controls was assessed upon DSS-induced colitis. Principal component analysis revealed no distinctive groups based on the genotype and no differentially abundant lipids were detected upon DSS-induced colitis (Figure S6C-D). However, the serum lipidome shifted upon DSS-induced colitis, reflecting the state of inflammation (Figure S6E). Overall, our data suggests that adipocyte autophagy controls the release of FFA upon TNFα stimulation and that its loss reduces systemic FFA levels *in vivo*.

Next, we wanted to address whether the reduction in FFA availability affects their uptake by immune cells in the adipose tissue or at the site of inflammation. Medium and long chain fatty acids are taken up through the fatty acid transporter CD36, which is expressed on multiple cell types, including immune cells. Thus, we assessed the expression of CD36 *in vivo* to identify immune cell subsets that acquire FFA in their tissue environment upon DSS-induced colitis. In the colon, CD36 expression on lymphocytes and monocytes was reduced upon DSS colitis, whereas its expression on dendritic cells and macrophages remained unchanged (Figure S6F). Interestingly, ATMs increased their expression of CD36 upon DSS-induced colitis, which was blunted on ATMs isolated from DSS-treated *Atg7*^{Ad} mice in mesenteric and visceral adipose tissues (Figure 5G). This is in line with previous reports demonstrating that CD36 is upregulated on ATMs upon increased adipose tissue lipolysis in mice submitted to caloric restriction (Kosteli et al., 2010). Taken together, our data implicates adipocyte autophagy in the provision of FFA, both systemically and locally, resulting in altered FFA transporter expression by ATMs.

Adipocyte autophagy controls IL-10 secretion from mesenteric and visceral adipose tissues upon DSS-induced colitis

Fatty acid availability can have a significant functional impact on immune cells (Rosa Neto et al., 2021). Next, we tested whether the autophagy-dependent decrease in adipose tissue lipolysis resulted in differentially secreted cytokines from ATMs. To address this, we screened the serum using a pre-defined inflammatory cytokine panel. Strikingly, while IL-10 and IL-27 were significantly upregulated in

484 DSS-treated wild type mice, their expression was diminished in adipocyte autophagy-deficient mice
485 (Figure 6A). The difference in IL-10 levels in the serum did not arise from the colon, since only *Il27*
486 transcript levels, but not *Il10*, were increased in the lamina propria of *Atg7*^{Ad} mice upon colitis induction
487 (Figure 6B).
488 It has been previously described that adipose tissue immune cells can increase expression of IL-10
489 upon intestinal inflammation (Kredel et al., 2013) . Unbiased cytokine screening of secreted cytokines
490 from wild-type mice revealed that several cytokines are released from the mesenteric adipose tissue in
491 response to both DSS- and *Hh*-induced colitis (Figure S7A-D). Importantly, and validating previous
492 reports, IL-10 secretion from the mesenteric adipose tissue was significantly up-regulated at peak
493 inflammation of DSS-induced colitis (Figure 6C). We therefore tested whether IL-10 secretion from the
494 mesenteric and gonadal adipose tissue was affected by adipocyte autophagy loss. Remarkably,
495 disruption of adipocyte autophagy abolished DSS-induced IL-10 secretion from both mesenteric and
496 gonadal adipose tissues, indicating that even adipose tissues that are not adjacent to the inflammation
497 site contribute to the anti-inflammatory response (Figure 6D). This response was consistent with
498 decreased systemic IL-10 levels in the serum (Figure 6A). Adipose tissue inflammation is associated
499 with an increase in TNFα secretion during obesity, promoting metaflammation (Sethi and Hotamisligil,
500 2021). However, loss of adipocyte autophagy did not lead to an increased secretion of TNFα from
501 adipose tissues (Figure 6E), thus demonstrating that adipose tissue inflammation is not responsible for
502 increased systemic TNFα levels. TNFα is most likely produced by the colon under the influence of
503 reduced systemic IL-10. Taken together, adipose tissues augment cytokine secretion during intestinal
504 inflammation, actively contributing to systemic cytokine production. Furthermore, our data suggest that
505 adipocyte autophagy regulates IL-10 production from both mesenteric and visceral adipose tissues.
506
507 *FFA restriction impairs IL-10 production in macrophages*
508 Next, to determine which cells are the main source of IL-10 in adipose tissues, immune cells were
509 isolated and their cytokine production capacity was measured. We found that, upon DSS-induced
510 colitis, F4/80^{+} macrophages are the main producers of IL-10 in mesenteric and visceral adipose tissues,
511 although CD4^{+} T cells appear to contribute as well in mesenteric WAT (Figure 7A). To directly confirm
512 whether local FFA availability can modify macrophage-derived IL-10 production, we sought to restrict

FFA availability from bone marrow derived macrophages. Charcoal treatment has previously been used to deplete FFAs from serum (Chen, 1967). First, we confirmed that FFA concentrations in medium containing charcoal-treated FBS ($R_{Charcoal}$) or serum-free medium (R_0) were reduced (Figure 7B). Culturing LPS and IFNγ stimulated macrophages in FFA-depleted medium blunted CD36 upregulation (Figure 7C), which correlated with medium FFA concentration (Figure 7D). Importantly, limiting FFA availability led to an increased proportion of TNFα-producing macrophages after 16h hours, while IL-10 producing cells were drastically reduced (Figure 7E). This indicated that FFA restriction leads to a sustained pro-inflammatory macrophage phenotype. In line with this, supernatant concentrations of IL-10 were clearly reduced upon FFA restriction (Figure 7F), thus indicating that local FFA availability impairs the production of anti-inflammatory IL-10 from macrophages.

Discussion

Inflammation and activation of immune cells promote intracellular metabolic adaptation, which is important to govern pro- and anti-inflammatory pathways (O'Neill et al., 2016). However, immune cells reside within distinct tissue environments and the impact of local nutrient availability on inflammatory processes remains incompletely understood (Richter et al., 2018). In this study, we demonstrate that autophagy in adipocytes promotes a cell-extrinsic effect on the secretion of IL-10 by adipose-tissue resident ATMs. Our results further indicate that autophagy in mature adipocytes is crucial for optimal cellular release and availability of FFA during inflammation. Autophagy-dependent IL-10 secretion from adipose tissue contributes to systemic levels, and limits inflammation at a distant tissue site, the intestine. Therefore, our study provides novel insights into a cross-tissue anti-inflammatory mechanism, enabling the development of alternative therapeutic approaches to treat inflammatory diseases.

Autophagy genes are well established as genetic risk factors for IBD susceptibility. Yet, little is known about the role of adipocyte autophagy in this disease. We found that autophagy is increased in visceral adipocytes upon DSS-induced colitis and showed that adipocytes transcriptionally increased the expression of several *Atg8* homologues during peak inflammation. These observations parallel findings during muscle atrophy, where the expression of *Map1lc3b, Gabarapl1, Bnip3, Bnip3l and Vps34* is regulated via FOXO3 activation, which subsequently controls autophagy levels (Mammucari et al.,

2007). It appears plausible that a similar FOXO3-dependent cachexia occurs in adipocytes. Interestingly, *Foxo3*-deficient mice develop more severe DSS-induced colitis than wild-type littermates (Snoeks et al., 2009). The induced genetic ablation of *Atg7* in mature adipocytes did not induce spontaneous colitis, thus indicating that genetic alterations in adipocyte autophagy by itself does not cause intestinal inflammation. However, adipocyte autophagy loss upon intestinal tissue damage worsened disease severity, pointing towards a supporting role of adipocyte autophagy in controlling immune exacerbation. We conclude that the involvement of autophagy in this pathology may depend on intestinal-derived cues (such as TNFα or bacterial translocation) and on a threshold to promote systemic inflammation (Rivera et al., 2019).

Detailed analysis of the visceral adipose secretome revealed that it is a prominent source of cytokines during intestinal inflammation. This work expands previous observations describing an increase of pro-inflammatory cytokine gene expression in mesenteric adipose tissues upon DSS-induced colitis (Mustain et al., 2013). Of note, the transcriptome of visceral adipocytes did not reveal changes in inflammatory cytokine expression upon DSS-treatment, thus indicating that the expression of these cytokines is likely derived from adipose tissue-resident immune cells. In addition to inflammatory cytokines, the secretion of IL-10 was observed in visceral adipose tissues upon intestinal inflammation, confirming findings from the Siegmund lab that mesenteric ATMs upregulate expression of IL-10 during intestinal inflammation in both human and mouse (Batra et al., 2012; Kredel et al., 2013). Importantly, this study underscores the importance of adipose-tissue derived IL-10 in controlling disease severity. Interestingly, we were unable to find differences in the *Hh*-induced colitis model. This may be explained by the administration of the IL-10R blocking antibody which neutralizes the anti-inflammatory effects of adipose tissue-derived IL-10 in this model of colitis, especially since we noted that IL-10 is actively secreted from *Hh* and IL10R-adipose tissues, thus suggesting that a similar pathway may also be present in this model of colitis. Recent single cell transcriptomic analysis of immune cells resident in creeping fat tissues revealed an important anti-inflammatory and pro-repair role of ATMs, further supporting their beneficial role during intestinal inflammation (Ha et al., 2020). Intriguingly, their study also identified a significant upregulation of IL-10 in ATMs in creeping fat tissue, suggesting that the adipocyte-immune cell pathway identified here is relevant for human IBD.

Early studies found that autophagy is crucial for adipogenesis and the normal differentiation of adipose tissues *in vivo* (Singh et al., 2009; Zhang et al., 2009). However, the significance of autophagy in mature adipocytes remained unexplored until recently. We propose that autophagy in mature adipocytes fine-tunes lipolytic output of adipocytes upon metabolic and/or inflammatory stress conditions. Supporting this view, post-developmental ablation of autophagy in mature adipocytes decreased β-adrenergic receptor-induced lipolysis (Cai et al., 2018; Son et al., 2020). Conversely, disruption of mTOR by genetic deletion of Raptor increases lipolytic output via autophagy (Zhang et al., 2020). While we were unable to observe signs of lipophagy by electron microscopy, it is possible that adipocyte autophagy controls lipolytic output via the degradation of key proteins involved in the lipolytic machinery such as described for perilipins in fibroblasts and adipocytes (Ju et al., 2019; Kaushik and Cuervo, 2016).

Macrophages accumulate in creeping fat tissues of CD patients and in the mesentery of mice upon DSS-induced colitis (Batra et al., 2012). We show that local FFA availability can dictate functional macrophage responses, such as the secretion of IL-10. In line with this, M2-type macrophages require uptake of lipid substrates through CD36 to engage OXPHOS-dependent cell activation (Huang et al., 2014). Even in iNKT cells and Tregs, the production of IL-10 can be regulated through the availability of FFA in the adipose tissue (LaMarche et al., 2020; Pompura et al., 2021). The importance of lipid metabolism for M2 polarization and function has further been demonstrated by the macrophage-specific loss of PPARγ and PPARδ (Odegaard et al., 2007; Odegaard et al., 2008). The resulting reduction in systemic IL-10 levels due to lipid restriction prolongs pro-inflammatory programs at the inflammation site. Especially, IL-10 signalling is required for intestinal macrophages to prevent excessive glycolytic and pro-inflammatory activity during DSS-induced colitis by inhibiting mTOR activity (Ip et al., 2017).

The importance of cell-extrinsic autophagy becomes increasingly apparent for intercellular and inter-tissue communication. While the exchange of nutrients, especially amino acids, has been predominantly characterized in the context of cancer (Poillet-Perez and White, 2019), it remained unclear whether it occurs in immunity. This report presents to our knowledge the first demonstration of an autophagy-dependent mobilization of lipids during inflammation. This is supported by an elegant

study suggesting that, during organ wasting, autophagy cell-extrinsically mobilizes stored nutrients to cancer cells to sustain their growth (Khezri et al., 2021). Despite its central function in bulk degradation and nutrient recycling, parts of the autophagic machinery have been implicated in other cell-extrinsic processes such as secretory autophagy and the release of extracellular vesicles (Kuramoto et al., 2021; Leidal et al., 2020; Nicolas-Avila et al., 2020). While we found that regulation of autophagy-dependent FFA levels can control IL-10 production in macrophages, we cannot exclude that other cell-extrinsic processes of autophagy may contribute to the observed phenotype.

Overall, this study reveals that metabolically healthy adipose tissues are important regulators of excessive inflammation during colitis. While visceral adipose tissues can adapt both pro- and anti-inflammatory properties, its impact on the pathology may depend on the overall disease state, genetic predispositions and co-morbidities. In this context, the expansion of the mesentery during CD may initially be beneficial through prevention of bacterial translocation and signalling pathways poised to promote anti-inflammatory and pro-fibrotic pathways (Batra et al., 2012; Ha et al., 2020). However, sustained inflammation may ultimately subvert the function of the mesentery and ultimately lead to adipose tissue fibrosis and intestinal strictures (Mao et al., 2019). Here, we demonstrate that adipocyte autophagy contributes cell-extrinsically to the provision of FFA and thus controls the anti-inflammatory immune response to intestinal tissue injury (see Graphical Abstract). It underlines the importance of local adipocyte-immune cell crosstalk through regulation of nutrient availability. This may present a broader local metabolic regulatory pathway to control immune responses to inflammation and infection.

Acknowledgements

We thank Patricia Cotta Moreira, Daniel Andrew and Mino Medghalchi from the Kennedy Institute animal facility for their excellent care and assistance of animal well-being. Dr. Nicholas Illot, Alina Janney and Dr. Luca Baù for their help with R coding. Discussions about experimental design for the transcriptomic experiments and sequencing were performed with help of Prof. Stephen Samson, Dr. Moustafa Attar and the Oxford Genomics Centre. Histology was performed with the help from the Kennedy Institute Histology Facility, especially Dr. Ida Parisi. This work was supported by grants from the Wellcome Trust (Investigator award 103830/Z/14/Z and 220784/Z/20/Z to A.K.S., Investigator award 212240/Z/18/Z to F.P., PhD studentship award 203803/Z16/Z to F.C.R., PhD studentship award 108869/Z/15/Z to S.K.W.), the Kenneth Rainin Foundation (Innovator award 20210017 to A.K.S. and F.P., jointly), the Kennedy Trust Studentship (KEN192001 to K.P.), the Marie Sklodowska-Curie - European Fellowship (893676 to M.B.) Blood Cancer UK (15026 and 17012 to C.M.E). Li-cor Odyssey imager was funded by ERC AdG 670930.

Authors Contribution

Conceptualization, F.C.R, M.F and K.A.S.; Methodology, F.C.R, M.F., I.G., E.J.; Formal Analysis, F.C.R. and M.F.; Investigation, F.C.R., M.F., M.P., G.A., I.G., S.K.W., E.J., M.B., K.P., P.H.; Writing – Original Draft, F.C.R., A.K.S; Writing – Review and Editing, M.F., M.P., G.A., I.G., S.K.W., E.J., M.B., K.P., P.H., H.S.S., C.M.E., A.K.S.; Visualization, F.C.R, Supervision, M.F., H.S.S., C.M.E, F.P., A.K.S.; Funding Acquisition, F.C.R., F.P., A.K.S.

Declaration of Interests

F.P. received research support or consultancy fees from Roche, Janssen, GSK, Novartis and Genentech. A,K.S. received consultancy fees from Calico, Oxford Healthspan, The Longevity Lab.

References

An, Y.A., and Scherer, P.E. (2020). Mouse Adipose Tissue Protein Extraction. Bio Protoc *10*, e3631.

Baazim, H., Antonio-Herrera, L., and Bergthaler, A. (2021). The interplay of immunology and cachexia in infection and cancer. Nat Rev Immunol.

Batra, A., Heimesaat, M.M., Bereswill, S., Fischer, A., Glauben, R., Kunkel, D., Scheffold, A., Erben, U., Kuhl, A., Loddenkemper, C*., et al.* (2012). Mesenteric fat - control site for bacterial translocation in colitis? Mucosal Immunol *5*, 580-591.

Bray, N.L., Pimentel, H., Melsted, P., and Pachter, L. (2016). Near-optimal probabilistic RNA-seq quantification. Nat Biotechnol *34*, 525-527.

Cadwell, K., Liu, J.Y., Brown, S.L., Miyoshi, H., Loh, J., Lennerz, J.K., Kishi, C., Kc, W., Carrero, J.A., Hunt, S*., et al.* (2008). A key role for autophagy and the autophagy gene Atg16l1 in mouse and human intestinal Paneth cells. Nature *456*, 259-263.

Cadwell, K., Patel, K.K., Komatsu, M., Virgin, H.W.t., and Stappenbeck, T.S. (2009). A common role for Atg16L1, Atg5 and Atg7 in small intestinal Paneth cells and Crohn disease. Autophagy *5*, 250-252.

Cai, J., Pires, K.M., Ferhat, M., Chaurasia, B., Buffolo, M.A., Smalling, R., Sargsyan, A., Atkinson, D.L., Summers, S.A., Graham, T.E*., et al.* (2018). Autophagy Ablation in Adipocytes Induces Insulin Resistance and Reveals Roles for Lipid Peroxide and Nrf2 Signaling in Adipose-Liver Crosstalk. Cell Rep *25*, 1708-1717 e1705.

Cawthorn, W.P., and Sethi, J.K. (2008). TNF-alpha and adipocyte biology. FEBS Lett *582*, 117-131.

Chen, R.F. (1967). Removal of fatty acids from serum albumin by charcoal treatment. J Biol Chem *242*, 173-181.

Clarke, A.J., and Simon, A.K. (2019). Autophagy in the renewal, differentiation and homeostasis of immune cells. Nat Rev Immunol *19*, 170-183.

Collins, K.H., Lenz, K.L., Pollitt, E.N., Ferguson, D., Hutson, I., Springer, L.E., Oestreich, A.K., Tang, R., Choi, Y.R., Meyer, G.A*., et al.* (2021). Adipose tissue is a critical regulator of osteoarthritis. Proc Natl Acad Sci U S A *118*.

Danne, C., Ryzhakov, G., Martinez-Lopez, M., Ilott, N.E., Franchini, F., Cuskin, F., Lowe, E.C., Bullers, S.J., Arthur, J.S.C., and Powrie, F. (2017). A Large Polysaccharide Produced by Helicobacter hepaticus Induces an Anti-inflammatory Gene Signature in Macrophages. Cell Host Microbe *22*, 733-745 e735.

Dieleman, L.A., Palmen, M.J., Akol, H., Bloemena, E., Pena, A.S., Meuwissen, S.G., and Van Rees, E.P. (1998). Chronic experimental colitis induced by dextran sulphate sodium (DSS) is characterized by Th1 and Th2 cytokines. Clin Exp Immunol *114*, 385-391.

Fischer, F.A., Mies, L.F.M., Nizami, S., Pantazi, E., Danielli, S., Demarco, B., Ohlmeyer, M., Lee, M.S.J., Coban, C., Kagan, J.C*., et al.* (2021). TBK1 and IKKepsilon act like an OFF switch to limit NLRP3 inflammasome pathway activation. Proc Natl Acad Sci U S A *118*.

Folch, J., Lees, M., and Sloane Stanley, G.H. (1957). A simple method for the isolation and purification of total lipides from animal tissues. J Biol Chem *226*, 497-509.

Friedrich, M., Pohin, M., and Powrie, F. (2019). Cytokine Networks in the Pathophysiology of Inflammatory Bowel Disease. Immunity *50*, 992-1006.

Grant, R.W., and Dixit, V.D. (2015). Adipose tissue as an immunological organ. Obesity (Silver Spring) *23*, 512-518.

Green, A., Dobias, S.B., Walters, D.J., and Brasier, A.R. (1994). Tumor necrosis factor increases the rate of lipolysis in primary cultures of adipocytes without altering levels of hormone-sensitive lipase. Endocrinology *134*, 2581-2588.

Guiboileau, A., Avila-Ospina, L., Yoshimoto, K., Soulay, F., Azzopardi, M., Marmagne, A., Lothier, J., and Masclaux-Daubresse, C. (2013). Physiological and metabolic consequences of autophagy deficiency for the management of nitrogen and protein resources in Arabidopsis leaves depending on nitrate availability. New Phytol *199*, 683-694.

Guiboileau, A., Yoshimoto, K., Soulay, F., Bataille, M.P., Avice, J.C., and Masclaux-Daubresse, C. (2012). Autophagy machinery controls nitrogen remobilization at the whole-plant level under both limiting and ample nitrate conditions in Arabidopsis. New Phytol *194*, 732-740.

Ha, C.W.Y., Martin, A., Sepich-Poore, G.D., Shi, B., Wang, Y., Gouin, K., Humphrey, G., Sanders, K., Ratnayake, Y., Chan, K.S.L.*, et al.* (2020). Translocation of Viable Gut Microbiota to Mesenteric Adipose Drives Formation of Creeping Fat in Humans. Cell *183*, 666-683 e617.

Hampe, J., Franke, A., Rosenstiel, P., Till, A., Teuber, M., Huse, K., Albrecht, M., Mayr, G., De La Vega, F.M., Briggs, J.*, et al.* (2007). A genome-wide association scan of nonsynonymous SNPs identifies a susceptibility variant for Crohn disease in ATG16L1. Nat Genet *39*, 207-211.

Ho, Y.T., Shimbo, T., Wijaya, E., Kitayama, T., Takaki, S., Ikegami, K., Miyashita, K., Ouchi, Y., Takaki, E., Yamamoto, R.*, et al.* (2021). Longitudinal Single-Cell Transcriptomics Reveals a Role for Serpina3n-Mediated Resolution of Inflammation in a Mouse Colitis Model. Cell Mol Gastroenterol Hepatol *12*, 547-566.

Hotamisligil, G.S. (2017). Inflammation, metaflammation and immunometabolic disorders. Nature *542*, 177-185.

Huang, S.C., Everts, B., Ivanova, Y., O'Sullivan, D., Nascimento, M., Smith, A.M., Beatty, W., Love-Gregory, L., Lam, W.Y., O'Neill, C.M.*, et al.* (2014). Cell-intrinsic lysosomal lipolysis is essential for alternative activation of macrophages. Nat Immunol *15*, 846-855.

Ip, W.K.E., Hoshi, N., Shouval, D.S., Snapper, S., and Medzhitov, R. (2017). Anti-inflammatory effect of IL-10 mediated by metabolic reprogramming of macrophages. Science *356*, 513-519.

Jostins, L., Ripke, S., Weersma, R.K., Duerr, R.H., McGovern, D.P., Hui, K.Y., Lee, J.C., Schumm, L.P., Sharma, Y., Anderson, C.A.*, et al.* (2012). Host-microbe interactions have shaped the genetic architecture of inflammatory bowel disease. Nature *491*, 119-124.

Ju, L., Han, J., Zhang, X., Deng, Y., Yan, H., Wang, C., Li, X., Chen, S., Alimujiang, M., Li, X.*, et al.* (2019). Obesity-associated inflammation triggers an autophagy-lysosomal response in adipocytes and causes degradation of perilipin 1. Cell Death Dis *10*, 121.

Kabat, A.M., Harrison, O.J., Riffelmacher, T., Moghaddam, A.E., Pearson, C.F., Laing, A., Abeler-Dorner, L., Forman, S.P., Grencis, R.K., Sattentau, Q.*, et al.* (2016). The autophagy gene Atg16l1 differentially regulates Treg and TH2 cells to control intestinal inflammation. Elife *5*, e12444.

Kang, Y.H., Cho, M.H., Kim, J.Y., Kwon, M.S., Peak, J.J., Kang, S.W., Yoon, S.Y., and Song, Y. (2016). Impaired macrophage autophagy induces systemic insulin resistance in obesity. Oncotarget *7*, 35577-35591.

Katheder, N.S., Khezri, R., O'Farrell, F., Schultz, S.W., Jain, A., Rahman, M.M., Schink, K.O., Theodossiou, T.A., Johansen, T., Juhasz, G.*, et al.* (2017). Microenvironmental autophagy promotes tumour growth. Nature *541*, 417-420.

Kaushik, S., and Cuervo, A.M. (2016). AMPK-dependent phosphorylation of lipid droplet protein PLIN2 triggers its degradation by CMA. Autophagy *12*, 432-438.

Khezri, R., Holland, P., Schoborg, T.A., Abramovich, I., Takats, S., Dillard, C., Jain, A., O'Farrell, F., Schultz, S.W., Hagopian, W.M., *et al.* (2021). Host autophagy mediates organ wasting and nutrient mobilization for tumor growth. EMBO J *40*, e107336.

Kojouharoff, G., Hans, W., Obermeier, F., Mannel, D.N., Andus, T., Scholmerich, J., Gross, V., and Falk, W. (1997). Neutralization of tumour necrosis factor (TNF) but not of IL-1 reduces inflammation in chronic dextran sulphate sodium-induced colitis in mice. Clin Exp Immunol *107*, 353-358.

Komatsu, M., Waguri, S., Ueno, T., Iwata, J., Murata, S., Tanida, I., Ezaki, J., Mizushima, N., Ohsumi, Y., Uchiyama, Y., *et al.* (2005). Impairment of starvation-induced and constitutive autophagy in Atg7-deficient mice. J Cell Biol *169*, 425-434.

Kosteli, A., Sugaru, E., Haemmerle, G., Martin, J.F., Lei, J., Zechner, R., and Ferrante, A.W., Jr. (2010). Weight loss and lipolysis promote a dynamic immune response in murine adipose tissue. J Clin Invest *120*, 3466-3479.

Kredel, L.I., Batra, A., Stroh, T., Kuhl, A.A., Zeitz, M., Erben, U., and Siegmund, B. (2013). Adipokines from local fat cells shape the macrophage compartment of the creeping fat in Crohn's disease. Gut *62*, 852-862.

Kuramoto, K., Kim, Y.J., Hong, J.H., and He, C. (2021). The autophagy protein Becn1 improves insulin sensitivity by promoting adiponectin secretion via exocyst binding. Cell Rep *35*, 109184.

LaMarche, N.M., Kane, H., Kohlgruber, A.C., Dong, H., Lynch, L., and Brenner, M.B. (2020). Distinct iNKT Cell Populations Use IFNgamma or ER Stress-Induced IL-10 to Control Adipose Tissue Homeostasis. Cell Metab *32*, 243-258 e246.

Leidal, A.M., Huang, H.H., Marsh, T., Solvik, T., Zhang, D., Ye, J., Kai, F., Goldsmith, J., Liu, J.Y., Huang, Y.H., *et al.* (2020). The LC3-conjugation machinery specifies the loading of RNA-binding proteins into extracellular vesicles. Nat Cell Biol *22*, 187-199.

Love, M.I., Huber, W., and Anders, S. (2014). Moderated estimation of fold change and dispersion for RNA-seq data with DESeq2. Genome Biol *15*, 550.

Mammucari, C., Milan, G., Romanello, V., Masiero, E., Rudolf, R., Del Piccolo, P., Burden, S.J., Di Lisi, R., Sandri, C., Zhao, J., *et al.* (2007). FoxO3 controls autophagy in skeletal muscle in vivo. Cell Metab *6*, 458-471.

Mao, R., Kurada, S., Gordon, I.O., Baker, M.E., Gandhi, N., McDonald, C., Coffey, J.C., and Rieder, F. (2019). The Mesenteric Fat and Intestinal Muscle Interface: Creeping Fat Influencing Stricture Formation in Crohn's Disease. Inflamm Bowel Dis *25*, 421-426.

McCarroll, S.A., Huett, A., Kuballa, P., Chilewski, S.D., Landry, A., Goyette, P., Zody, M.C., Hall, J.L., Brant, S.R., Cho, J.H., *et al.* (2008). Deletion polymorphism upstream of IRGM associated with altered IRGM expression and Crohn's disease. Nat Genet *40*, 1107-1112.

Mustain, W.C., Starr, M.E., Valentino, J.D., Cohen, D.A., Okamura, D., Wang, C., Evers, B.M., and Saito, H. (2013). Inflammatory cytokine gene expression in mesenteric adipose tissue during acute experimental colitis. PLoS One *8*, e83693.

Nicolas-Avila, J.A., Lechuga-Vieco, A.V., Esteban-Martinez, L., Sanchez-Diaz, M., Diaz-Garcia, E., Santiago, D.J., Rubio-Ponce, A., Li, J.L., Balachander, A., Quintana, J.A., *et al.* (2020). A Network of Macrophages Supports Mitochondrial Homeostasis in the Heart. Cell *183*, 94-109 e123.

Noti, M., Corazza, N., Mueller, C., Berger, B., and Brunner, T. (2010). TNF suppresses acute intestinal inflammation by inducing local glucocorticoid synthesis. J Exp Med *207*, 1057-1066.

O'Neill, L.A., Kishton, R.J., and Rathmell, J. (2016). A guide to immunometabolism for immunologists. Nat Rev Immunol *16*, 553-565.

Odegaard, J.I., Ricardo-Gonzalez, R.R., Goforth, M.H., Morel, C.R., Subramanian, V., Mukundan, L., Red Eagle, A., Vats, D., Brombacher, F., Ferrante, A.W.*, et al.* (2007). Macrophage-specific PPARgamma controls alternative activation and improves insulin resistance. Nature *447*, 1116-1120.

Odegaard, J.I., Ricardo-Gonzalez, R.R., Red Eagle, A., Vats, D., Morel, C.R., Goforth, M.H., Subramanian, V., Mukundan, L., Ferrante, A.W., and Chawla, A. (2008). Alternative M2 activation of Kupffer cells by PPARdelta ameliorates obesity-induced insulin resistance. Cell Metab *7*, 496-507.

Oliva, M., Munoz-Aguirre, M., Kim-Hellmuth, S., Wucher, V., Gewirtz, A.D.H., Cotter, D.J., Parsana, P., Kasela, S., Balliu, B., Vinuela, A.*, et al.* (2020). The impact of sex on gene expression across human tissues. Science *369*.

Poillet-Perez, L., and White, E. (2019). Role of tumor and host autophagy in cancer metabolism. Genes Dev *33*, 610-619.

Poillet-Perez, L., Xie, X., Zhan, L., Yang, Y., Sharp, D.W., Hu, Z.S., Su, X., Maganti, A., Jiang, C., Lu, W.*, et al.* (2018). Autophagy maintains tumour growth through circulating arginine. Nature *563*, 569-573.

Pompura, S.L., Wagner, A., Kitz, A., LaPerche, J., Yosef, N., Dominguez-Villar, M., and Hafler, D.A. (2021). Oleic acid restores suppressive defects in tissue-resident FOXP3 Tregs from patients with multiple sclerosis. J Clin Invest *131*.

Richter, F.C., Obba, S., and Simon, A.K. (2018). Local exchange of metabolites shapes immunity. Immunology *155*, 309-319.

Riffelmacher, T., Clarke, A., Richter, F.C., Stranks, A., Pandey, S., Danielli, S., Hublitz, P., Yu, Z., Johnson, E., Schwerd, T.*, et al.* (2017). Autophagy-Dependent Generation of Free Fatty Acids Is Critical for Normal Neutrophil Differentiation. Immunity *47*, 466-480 e465.

Riffelmacher, T., Richter, F.C., and Simon, A.K. (2018). Autophagy dictates metabolism and differentiation of inflammatory immune cells. Autophagy *14*, 199-206.

Rivera, E.D., Coffey, J.C., Walsh, D., and Ehrenpreis, E.D. (2019). The Mesentery, Systemic Inflammation, and Crohn's Disease. Inflamm Bowel Dis *25*, 226-234.

Rosa Neto, J.C., Calder, P.C., Curi, R., Newsholme, P., Sethi, J.K., and Silveira, L.S. (2021). The Immunometabolic Roles of Various Fatty Acids in Macrophages and Lymphocytes. Int J Mol Sci *22*.

Russo, L., and Lumeng, C.N. (2018). Properties and functions of adipose tissue macrophages in obesity. Immunology *155*, 407-417.

Ryden, M., Dicker, A., van Harmelen, V., Hauner, H., Brunnberg, M., Perbeck, L., Lonnqvist, F., and Arner, P. (2002). Mapping of early signaling events in tumor necrosis factor-alpha -mediated lipolysis in human fat cells. J Biol Chem *277*, 1085-1091.

Sassmann, A., Offermanns, S., and Wettschureck, N. (2010). Tamoxifen-inducible Cre-mediated recombination in adipocytes. Genesis *48*, 618-625.

Sethi, J.K., and Hotamisligil, G.S. (2021). Metabolic Messengers: tumour necrosis factor. Nat Metab *3*, 1302-1312.

Sheehan, A.L., Warren, B.F., Gear, M.W., and Shepherd, N.A. (1992). Fat-wrapping in Crohn's disease: pathological basis and relevance to surgical practice. Br J Surg *79*, 955-958.

Singh, R., Xiang, Y., Wang, Y., Baikati, K., Cuervo, A.M., Luu, Y.K., Tang, Y., Pessin, J.E., Schwartz, G.J., and Czaja, M.J. (2009). Autophagy regulates adipose mass and differentiation in mice. J Clin Invest *119*, 3329-3339.

Snoeks, L., Weber, C.R., Wasland, K., Turner, J.R., Vainder, C., Qi, W., and Savkovic, S.D. (2009). Tumor suppressor FOXO3 participates in the regulation of intestinal inflammation. Lab Invest *89*, 1053-1062.

Son, Y., Cho, Y.K., Saha, A., Kwon, H.J., Park, J.H., Kim, M., Jung, Y.S., Kim, S.N., Choi, C., Seong, J.K.*, et al.* (2020). Adipocyte-specific Beclin1 deletion impairs lipolysis and mitochondrial integrity in adipose tissue. Mol Metab *39*, 101005.

Sousa, C.M., Biancur, D.E., Wang, X., Halbrook, C.J., Sherman, M.H., Zhang, L., Kremer, D., Hwang, R.F., Witkiewicz, A.K., Ying, H.*, et al.* (2016). Pancreatic stellate cells support tumour metabolism through autophagic alanine secretion. Nature *536*, 479-483.

Stranks, A.J., Hansen, A.L., Panse, I., Mortensen, M., Ferguson, D.J., Puleston, D.J., Shenderov, K., Watson, A.S., Veldhoen, M., Phadwal, K.*, et al.* (2015). Autophagy Controls Acquisition of Aging Features in Macrophages. J Innate Immun *7*, 375-391.

Surma, M.A., Herzog, R., Vasilj, A., Klose, C., Christinat, N., Morin-Rivron, D., Simons, K., Masoodi, M., and Sampaio, J.L. (2015). An automated shotgun lipidomics platform for high throughput, comprehensive, and quantitative analysis of blood plasma intact lipids. Eur J Lipid Sci Technol *117*, 1540-1549.

Wang, L., Ray, A., Jiang, X., Wang, J.Y., Basu, S., Liu, X., Qian, T., He, R., Dittel, B.N., and Chu, Y. (2015). T regulatory cells and B cells cooperate to form a regulatory loop that maintains gut homeostasis and suppresses dextran sulfate sodium-induced colitis. Mucosal Immunol *8*, 1297-1312.

Whibley, N., Tucci, A., and Powrie, F. (2019). Regulatory T cell adaptation in the intestine and skin. Nat Immunol *20*, 386-396.

Wu, T., Hu, E., Xu, S., Chen, M., Guo, P., Dai, Z., Feng, T., Zhou, L., Tang, W., Zhan, L.*, et al.* (2021). clusterProfiler 4.0: A universal enrichment tool for interpreting omics data. Innovation (N Y) *2*, 100141.

Zhang, H., Alsaleh, G., Feltham, J., Sun, Y., Napolitano, G., Riffelmacher, T., Charles, P., Frau, L., Hublitz, P., Yu, Z.*, et al.* (2019). Polyamines Control eIF5A Hypusination, TFEB Translation, and Autophagy to Reverse B Cell Senescence. Mol Cell *76*, 110-125 e119.

Zhang, X., Wu, D., Wang, C., Luo, Y., Ding, X., Yang, X., Silva, F., Arenas, S., Weaver, J.M., Mandell, M.*, et al.* (2020). Sustained activation of autophagy suppresses adipocyte maturation via a lipolysis-dependent mechanism. Autophagy *16*, 1668-1682.

Zhang, Y., Goldman, S., Baerga, R., Zhao, Y., Komatsu, M., and Jin, S. (2009). Adipose-specific deletion of autophagy-related gene 7 (atg7) in mice reveals a role in adipogenesis. Proc Natl Acad Sci U S A *106*, 19860-19865.

Figure 1: DSS-induced intestinal inflammation promotes autophagy in adipose tissues.
(A) Schematic of experimental design. Sex-matched and age-matched wild-type mice were treated for 5 days with 1.5-2% DSS in drinking water, before switched to water for two more days. Mice were sacrificed at day 7 post-DSS induction.
(B) Body weight development upon DSS treatment; n = 10-11/group, pooled from three independent experiments.
(C) Tissue weights measured in mesenteric (mWAT) and collective visceral white adipose tissue (visWAT), consisting of gonadal (gWAT), retroperitoneal and omental white adipose tissue at day 7 after start of DSS regime; n = 7-8/group pooled from two independent experiments.
(D) Circulating serum levels of FFA during DSS-induced colitis at day 7; n = 15/group pooled from four independent experiments.
(E) Immunoblot analysis of autophagic flux in mWAT (upper panel) and gWAT (lower panel) adipose tissue stimulated *ex vivo* with lysosomal inhibitor 100nM Bafilomycin A1 and 20mM NH_4Cl for 4 hours or DMSO (Vehicle); n = 3-4/group pooled from two independent experiments.
(F) Representative transmission electron microscopy images from mesenteric adipose tissue 7 days post DSS-induced colitis induction. Lower panel is showing magnification of selected area. White arrows show autophagosomal structures.
(G) ATG8 homologues expression was measured by qPCR in visceral adipocytes fraction (right) and stromal vascular fraction (left panel) during DSS-induced colitis.; n = 7-8/group pooled from two independent experiment.

Data are represented as mean ± SEM. (B,G) Two-Way ANOVA. (C) Multiple unpaired t-test. (D,E) Unpaired Student's t-test.

Figure 2: Loss of adipocyte autophagy does neither alter systemic nor intestinal immune homeostasis.
(A) Schematic of experimental design. Sex-matched and age-matched littermates were treated at 8-12 weeks of age with tamoxifen for five consecutive days before tissues were analysed 14 days after the last tamoxifen administration.
(B) Representative quantification of knock-out efficiency measured on *Atg7* transcript level by qRT-PCR in purified primary visceral adipocyte at two weeks post-tamoxifen treatment (n = 4-11/group).
(C) Representative immunoblot for ATG7 and LC3-I/II protein expression and quantification of LC3 conversion ratio (LC3-II/LC3-I) (n = 3-10/group).
(D) Colon length after two weeks post-deletion; n = 14 pooled from two independent experiments.
(E) Representative H&E staining images (10x magnification) of colon sections and quantification; n = 9 from one independent experiment.
(F) Percentage (left panel) and absolute number of $CD45^+$ immune cells (right panel) from colons after two weeks post-deletion; n = 13-14 pooled from two independent experiments.
(G) Frequency of myeloid cell populations (left panel) and lymphoid populations (right panel) from colons after two weeks post-deletion; n = 13-14 pooled from two independent experiments.
(H) Frequency of $CD4^+$ T cell subpopulations from colons after two weeks post-deletion; n = 13-14 pooled from two independent experiments.

Data are represented as mean ± SEM. (B,C,G,H) Two-Way ANOVA. (D,E,F) Unpaired Student's t-test.

Figure 3: Loss of adipocyte autophagy exacerbates DSS-induced colitis.
(A) Schematic of experimental design. Sex-matched and age-matched littermates were treated at 8-12 weeks of age with tamoxifen for five consecutive days and DSS-induced colitis was induced after a two-week washout phase.
(B) Body weight development upon DSS treatment; n = 25 pooled from three independent experiments.
(C) Representative image of colon length from DSS-induced colitis mice and its quantification from non-inflamed control mice (n = 3-4) and adipocyte autophagy-sufficient WT mice and adipocyte autophagy-deficient mice; n = 18-22/group pooled from three independent experiments.

(D) Representative H&E staining images (10x magnification) of distal colon sections and quantification split by colon side (left panel) and scoring class (right panel) in non-inflamed control mice (n = 4), colitic WT mice and adipocyte autophagy-deficient *Atg7*^{Ad} mice; n = 18-22/group pooled from three independent experiments.
(E) Expression of pro-inflammatory cytokines in lamina propria at 7 days post-DSS induction; n = 18-22/group pooled from three independent experiments.
(F) Absolute number of immune cells present in the colon at day 7 post-DSS induction; n = 18-22/group pooled from three independent experiments.
(G) Frequency of myeloid cell population in colon at day 7 post-DSS induction; n = 18-22/group pooled from three independent experiments.
(H) Absolute number of Ly6C^{+} monocytes discriminated by the absence or presence of MHCII for infiltrating and inflammatory monocytes respectively; n = 18-22/group pooled from three independent experiments.

Data are represented as mean ± SEM. (B,C,G,H) Two-Way ANOVA. (D,E,F) Unpaired Student's t-test.

Figure 4: Intestinal inflammation promotes autophagic and fatty acid metabolic transcriptional programs in primary adipocytes.
(A) Schematic overview. Three female and three male mice were either kept on water or treated with DSS for seven days. Visceral adipose tissues were collected and digested. Floating adipocyte fraction was collected and sequenced for transcriptional profiling.
(B) Principal component analysis of all mice revealing a strong sex effect in the overall transcriptome.
(C) Pathway enrichment analysis of significantly differentially expressed genes in visceral adipocytes during DSS colitis.
(D) Heatmap representing differentially expressed genes associated with macroautophagy during DSS-induced colitis in visceral adipocytes.
(E) Heatmap representing differentially expressed genes associated in fatty acid metabolism during DSS-induced colitis in visceral adipocytes.
(F) Normalized counts of selected key enzymes and proteins involved in the lipolysis pathway in visceral adipocytes; n = 12/group.

Data are represented as mean ± SEM. (F) Unpaired Student's t-test.

Figure 5: Autophagy-deficient adipocytes differentially secrete fatty acids in response to TNFα
(A) Expression of the gene encoding TNF receptor 1, *Tnfrsf1a*, on visceral adipocytes during intestinal inflammation. Data expressed as normalized counts from transcriptome analysis.
(B) TNFα levels in serum were measured in wild-type mice at day 7 after water and DSS treatment.
(C) *Ex vivo* lipolysis assay on *Atg7*-deficient adipose tissue explants simulated with TNFα (100ng/mL) for 24h before replacing with fresh medium in the absence of TNFα for 3h; n = 4 representative for two independent experiments.
(D) Serum levels of circulating FFAs measured in wild-type and *Atg7*-deficient mice; n = 13-14 pooled from two independent experiments.
(E) Fraction of major FFA species in mouse serum in water-treated and DSS-treated mice; n = 12-14 pooled from two-three independent experiments.
(F) Fold change differences in serum quantities of FFA species in water-treated and DSS-treated mice; n = 12-14 pooled from two-three independent experiments.
(G) Representative plots of CD36 expression on adipose tissue macrophages isolated from mesenteric or visceral adipose tissues at day 7 after DSS-treatment. Representative for three independent experiments.

Data are represented as mean ± SEM. (B,C,E,F,G) Two-Way ANOVA. (A,D) Unpaired Student's t-test.

Figure 6: Adipocyte autophagy controls IL-10 secretion from mesenteric and visceral adipose tissues upon DSS-induced colitis

(A) Serum cytokines upon DSS-induced colitis at day 7 post-induction; n = 17-23/group pooled from three independent experiments.

(B) Expression of cytokines in lamina propria measured by qRT-PCR at 7 days post-DSS induction; n = 20-24/group pooled from three independent experiments.

(C) Colitis was induced in mice for 7 days and mesenteric adipose tissue explants were cultured with FBS. IL-10 secretion into the supernatant was measured after 24h of culture; n = 4-12/group pooled from two independent experiments.

(D and E) Colitis was induced in mice for 7 days and adipose tissues were extracted and cultured for 6 hours in serum-starved medium. Secretion of (D) IL-10 and (E) TNFα from mesenteric (left panel) and gonadal adipose tissues (right panel) was measured by ELISA. Shapes identify individual experiments; n = 5-15/group pooled from two independent experiments.

(F) Identification of IL-10-producing cells in adipose tissue upon DSS-induced colitis by flow cytometry. Representative FACS plots (left panel) and quantification from mesenteric (middle panel) and visceral adipose tissues (right panel); n = 7-9/group pooled from two independent experiments.

(G) Identification of IL-10 producing cells in adipose tissues of WT and *Atg7*^{Ad} mice upon DSS-induced colitis at day 7. Representative FACS plots (left panel) and quantification from mesenteric (middle panel) and visceral adipose tissue (right panel); n = 3-9/group from one independent experiment.

Data are represented as mean ± SEM. (A,F) Two-Way ANOVA. (B) One-Way ANOVA. (D,E) Two-Way ANOVA with regression for experiment. (C) Unpaired Student's t-test.

Figure 7: FFA restriction impairs IL-10 production in macrophages.

(A) Measuring FFA content in either full medium supplemented with 10% FBS (R_{10}), or without FBS (R_0), or with 10% Charcoal-treated FBS ($R_{Charcoal}$); n = 5/group pooled from two independent experiments.

(B) Bone marrow derived macrophages were differentiated for 7 days in M-CSF until polarized using LPS and IFNγ. Surface expression of fatty acid uptake transporter CD36 on M0 or M1 polarized macrophages; n = 4/group representative for three independent experiments.

(C) Correlation of CD36 surface expression and medium FFA concentration; n = 4 pooled from two independent experiments.

(D) Bone marrow derived macrophages were polarized in M-CSF or LPS/IFNγ for 16 hours, before stimulated with PMA/Ionomycin. TNFα (upper panel) and IL-10 (lower panel) production was measured after 4 hours of PMA/ionomycin stimulation by flow cytometry; n = 3-4/group representative for two independent experiments.

(E) Secreted cytokines into culture supernatant were measured by ELISA 16 hours after macrophage polarization with M-CSF or LPS/IFNγ.

Data are represented as mean ± SEM. (A) One-Way ANOVA. (B,D,E) Two-Way ANOVA. (C) Linear regression.

Supplementary Figure 1: Low DSS concentration leads to efficient induction of intestinal inflammation.
(A) Representative H&E staining of colon histology and quantification at day 7 after DSS colitis induction; n=3/group, representative for one experiment
(B) Colon length measured after 1.5-2% DSS colitis regime at day 7; n=6-7 pooled from two experiments
(C) Spleen weight and mesenteric lymph node weight after 1.5% colitis regime at day 7; n=9/group pooled from three experiments
(D) Absolute number of colonic $CD45^+$ immune cells at day 7 post-DSS treatment; n=6-7 pooled from two experiments.
(E) Frequency of $CD11b^+$ myeloid cells, $CD3^+$ T cells and $CD19^+$ B cells in colon at day 7 post-DSS treatment; n=6-7 pooled from two experiments.

Data are represented as mean ± SEM. (A,B,D,E) Unpaired Student's t-test. (C) Multiple t-test.

Supplementary Figure 2: Adipose tissue immune homeostasis is maintained despite loss of adipocyte autophagy.
(A) Body weight development upon tamoxifen treatment; n=10-11/group pooled from two independent experiments.
(B) Weight of mWAT and collective visWAT divided per sex two weeks after tamoxifen treatment; n=10-11/group pooled from two independent experiments.
(C) Gating strategy of adipose tissue myeloid cells.
(D) Frequency of $CD45^+$ immune cells in mesenteric and visceral adipose tissues two weeks after tamoxifen treatment; n=10-11/group pooled from two independent experiments.
(E) Frequency of myeloid cell populations two weeks after tamoxifen treatment in mesenteric and visceral adipose tissues; n=10-11/group pooled from two independent experiments.
(F) Gating strategy of adipose tissue lymphoid cells.
(G) Frequency of lymphoid cell populations two weeks after tamoxifen treatment in mesenteric and visceral adipose tissues; n=10-11/group pooled from two independent experiments.
(H) Frequency of T cell subsets two weeks after tamoxifen treatment in mesenteric and visceral adipose tissues; n=10-11/group pooled from two independent experiments.

Data are represented as mean ± SEM. (A-B, D-E,G-H) Two-Way ANOVA.

Supplementary Figure 3: Expansion of intestinal Treg populations is blunted in adipocyte autophagy-deficient mice without affecting intestinal resolution.
(A) Schematic of experimental design. Sex-matched and age-matched littermates were treated with DSS for five days and mice were sacrificed 14 days after start of DSS treatment.
(B) Colon length from non-inflamed control mice (n = 8), adipocyte autophagy-sufficient WT mice and adipocyte autophagy-deficient mice (n = 12), pooled from two independent experiments.
(C) Representative H&E staining images (10x magnification) of distal colon sections and quantification of histopathological score; n=7-13 pooled from two independent experiment.
(D) Frequency (left panel) and absolute number (right panel) of $CD4^+$ $FOXP3^+$ cells in the colon at day 14 post-DSS treatment; n = 8-11 pooled from two independent experiments.
(E) Frequency of peripheral and thymic Treg (pTreg and tTreg, respectively) cell populations in colon at day 14 post-DSS treatment; n = 6-11 pooled from two independent experiments.

Data are represented as mean ± SEM. (B-D) Two-Way ANOVA. (E) One-Way ANOVA.

Supplementary Figure 4: Loss of adipocyte autophagy does not alter Helicobacter hepaticus-induced intestinal inflammation.
(A) Schematic of experimental design. Sex-matched and age-matched littermates were treated with *Hh* and anti-IL10 receptor antibody 14 days after last tamoxifen administration. *Hh* was administered at the one day and anti-IL10 receptor seven days after the first administration. Colitis was assessed after two weeks (inflammation timepoint) and after six weeks (resolution timepoint).

(B) Representative H&E staining images (10x magnification) of distal colon sections and quantification of histopathological score; n=4-14/group pooled from two independent experiments.
(C) Absolute number of CD45+ immune cells in lamina propria 14 days after induction of colitis; n = 7-13/group pooled from two independent experiments.
(D) Frequency of immune cell populations in the lamina propria 14 days after induction of colitis; n = 7-13/group pooled from two independent experiments.
(E) Absolute number of T cell populations in the lamina propria 14 days after induction of colitis; n = 7-13/group pooled from two independent experiments.
(F) Absolute number of CD45+ immune cells in lamina propria 6 weeks after induction of colitis; n = 4-13/group pooled from two independent experiments.
(G) Frequency of immune cell populations in the lamina propria 6 weeks after induction of colitis; n = 4-13/group pooled from two independent experiments.
(H) Absolute number of T cell populations in the lamina propria 6 weeks after induction of colitis; n = 4-13/group pooled from two independent experiments.

Data are represented as mean ± SEM. (B,D-E,G) Two-Way ANOVA, (F) One-Way ANOVA.

Supplementary Figure 5: Limited impact of Atg7 deficiency on transcriptional profile in visceral adipocytes.
(A) Differential gene expression in visceral adipocytes from water-treated WT and *Atg7*^{Ad} animals two weeks after tamoxifen treatment.
(B) Differential gene expression in visceral adipocytes from DSS-treated WT and *Atg7*^{Ad} animals at day 7 post-DSS treatment.
(C) Differential gene expression assessing transcriptional changes associated with DSS-induced inflammation after regressing effect of sex and genotypes in visceral adipocytes.
(D) Normalized counts of selected Atg8 homologues in visceral adipocytes 7 days after induction of colitis; n = 12/group.

Data are represented as mean ± SEM. (D) Unpaired Student's t-test.

Supplementary 6: Systemic lipid homeostasis and intestinal CD36 expression remain largely unaltered in adipocyte autophagy-deficient mice during DSS-induced colitis.
(A) *Ex vivo* lipolysis assays on *Atg7*-deficient adipose tissue explants simulated with isoproterenol (10μM) for 1-2h; n = 4-5/group representative for three independent experiments.
(B) Gene expression of cytosolic lipases in visceral adipocytes upon DSS-induced colitis.
(C) Principal component analysis of serum lipidome of DSS-treated mice; n=5-6/group pooled from two independent experiments.
(D) Differentially expressed lipids in serum of DSS-treated mice before FDR correction (in black) and after FDR correction (in red); n=5-6/group pooled from two independent experiments.
(E) Principal component analysis of serum lipidome of water vs. DSS-treated mice; n=11-12/group pooled from two independent experiments.
(F) Expression of CD36 was measured by flow cytometry at day 7 post-DSS induction on intestinal immune cells; n = 6-10/group pooled from two independent experiments.

Data are represented as mean ± SEM. (A) Two-Way ANOVA. (B) Unpaired Student's t-test. (F) One-Way ANOVA.

Supplementary Figure 7: Mesenteric adipose tissues alter their cytokine profile upon DSS- and Hh-induced colitis in wild-type animals.
Secreted cytokines from wild-type mWAT cultured in medium containing 5% FBS for 24h which are (A) increased to a similar degree in both DSS- and *Hh*-induced colitis, (B) increased specifically in *Hh*-induced colitis, (C) increased in both colitis models, but more significantly in *Hh*-induced colitis and (D) not induced at all.

Data are represented as mean ± SEM. Statistical analysis by One-Way ANOVA from one (*Hh*) and two (DSS) independent experiments; each datapoint is one biological replicate.

Figure 1

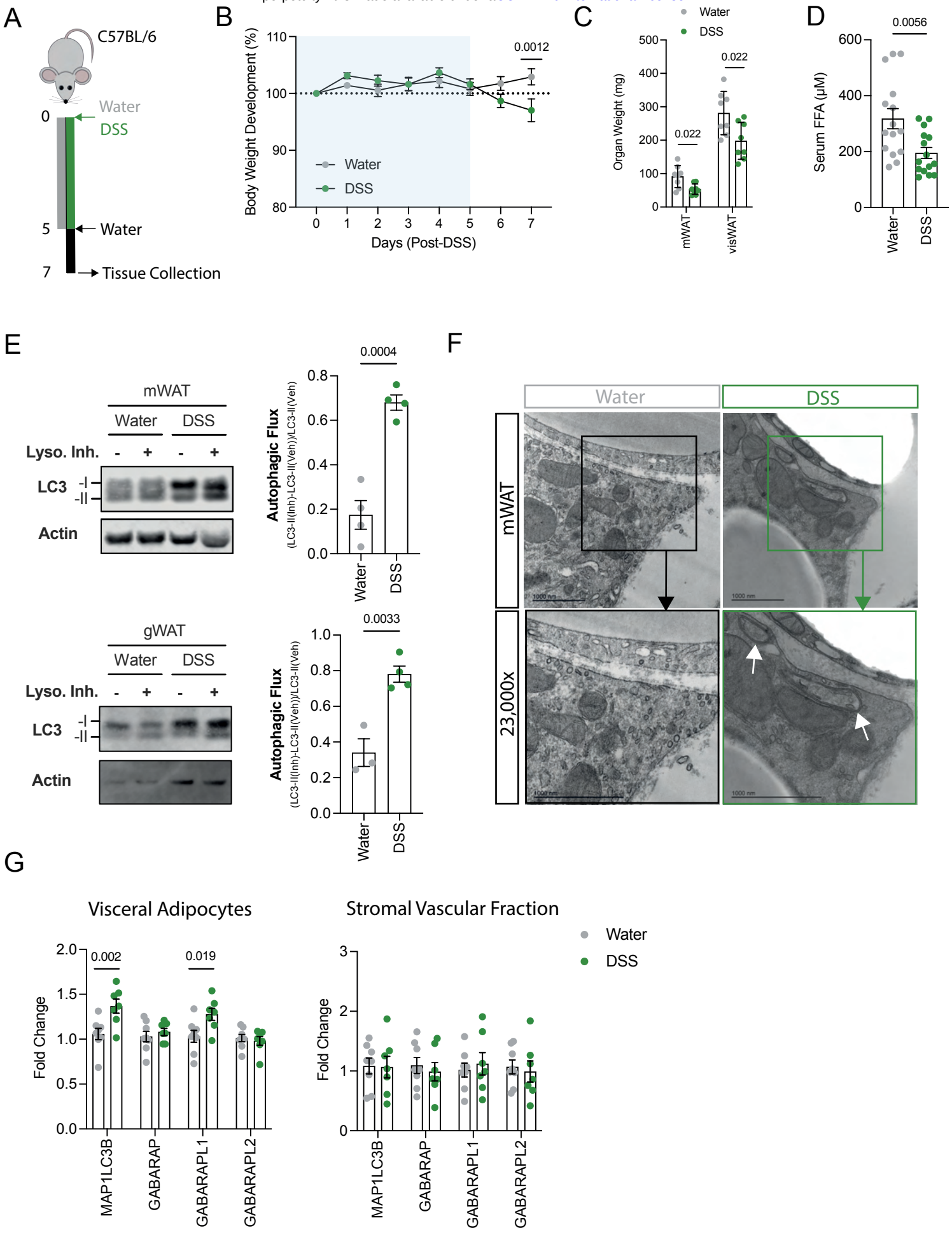

Figure 2

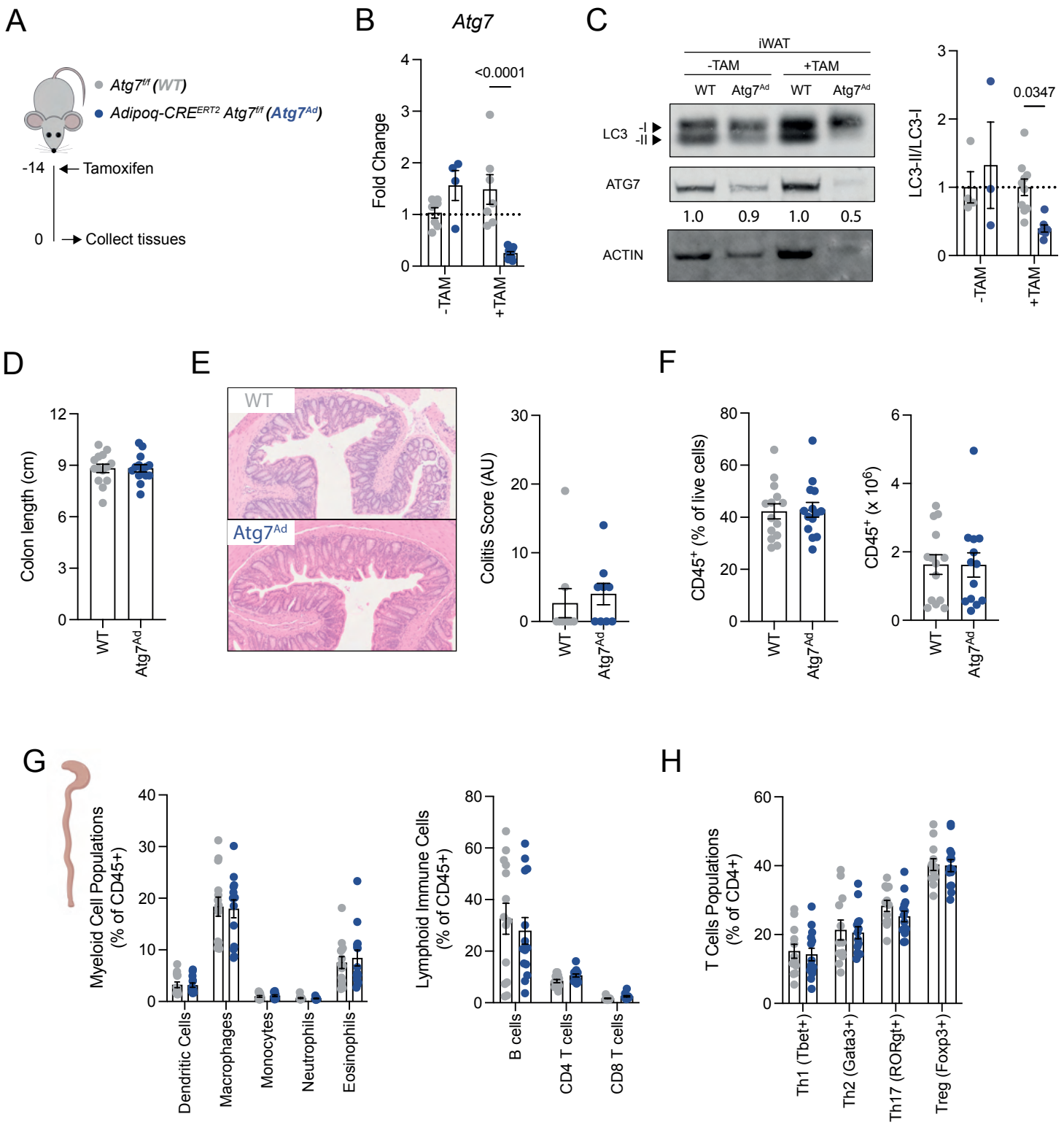

Figure 3

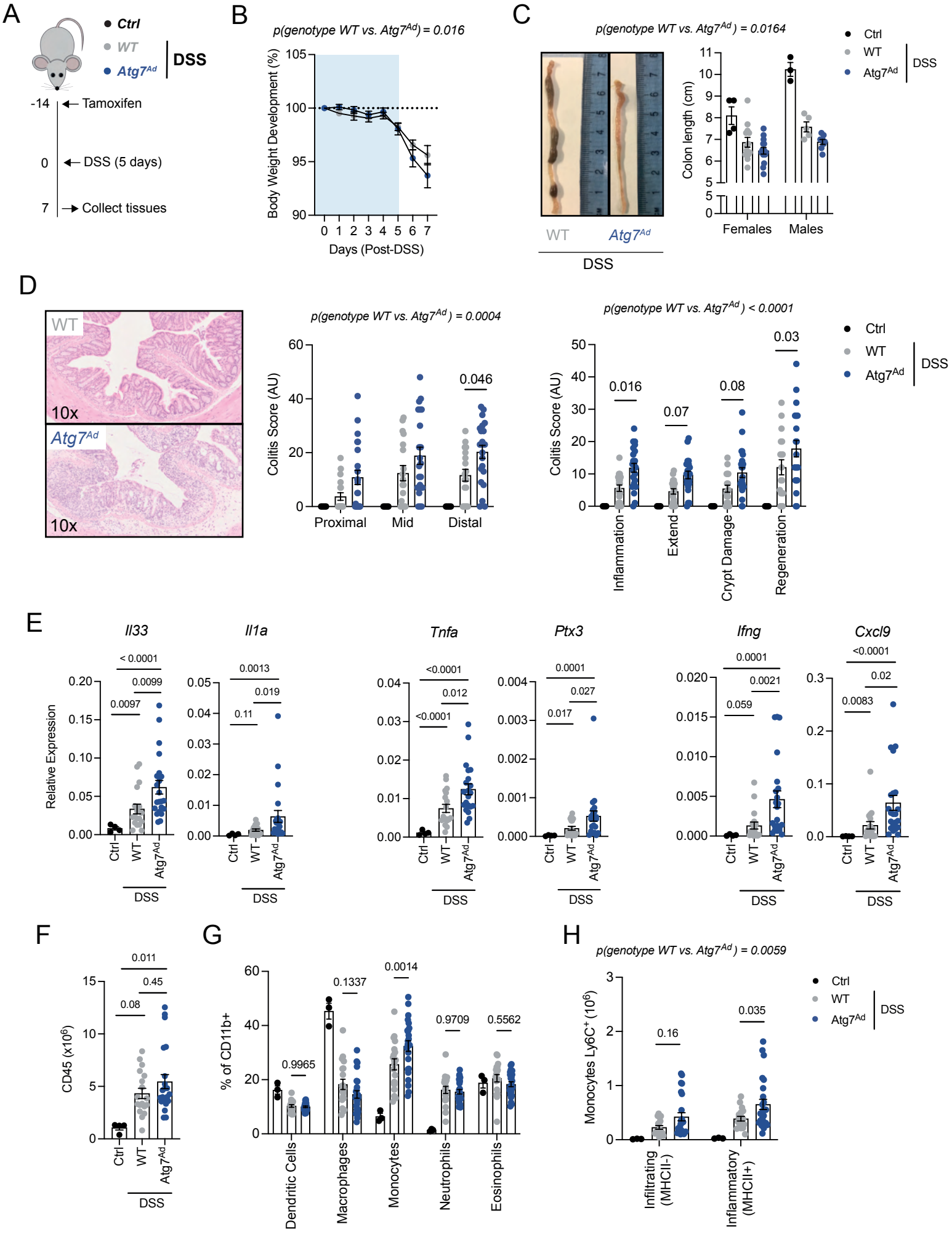
A
Ctrl
WT
Atg7Ad
DSS
-14
Tamoxifen
0
DSS (5 days)
7
Collect tissues
B
p(genotype WT vs. Atg7Ad) = 0.016
Body Weight Development (%)
Days (Post-DSS)
C
p(genotype WT vs. Atg7Ad) = 0.0164
Colon length (cm)
Females
Males
WT
Atg7Ad
DSS
D
WT
Atg7Ad
10x
p(genotype WT vs. Atg7Ad) = 0.0004
Colitis Score (AU)
Proximal
Mid
Distal
0.046
p(genotype WT vs. Atg7Ad) < 0.0001
0.016
0.07
0.08
0.03
Inflammation
Extend
Crypt Damage
Regeneration
E
Il33
Il1a
Tnfa
Ptx3
Ifng
Cxcl9
Relative Expression
F
CD45 (x10^6)
0.011
0.45
0.08
G
% of CD11b+
0.9965
0.1337
0.0014
0.9709
0.5562
Dendritic Cells
Macrophages
Monocytes
Neutrophils
Eosinophils
H
p(genotype WT vs. Atg7Ad) = 0.0059
Monocytes Ly6C+ (10^6)
0.16
0.035
Infiltrating (MHCII-)
Inflammatory (MHCII+)

Figure 4

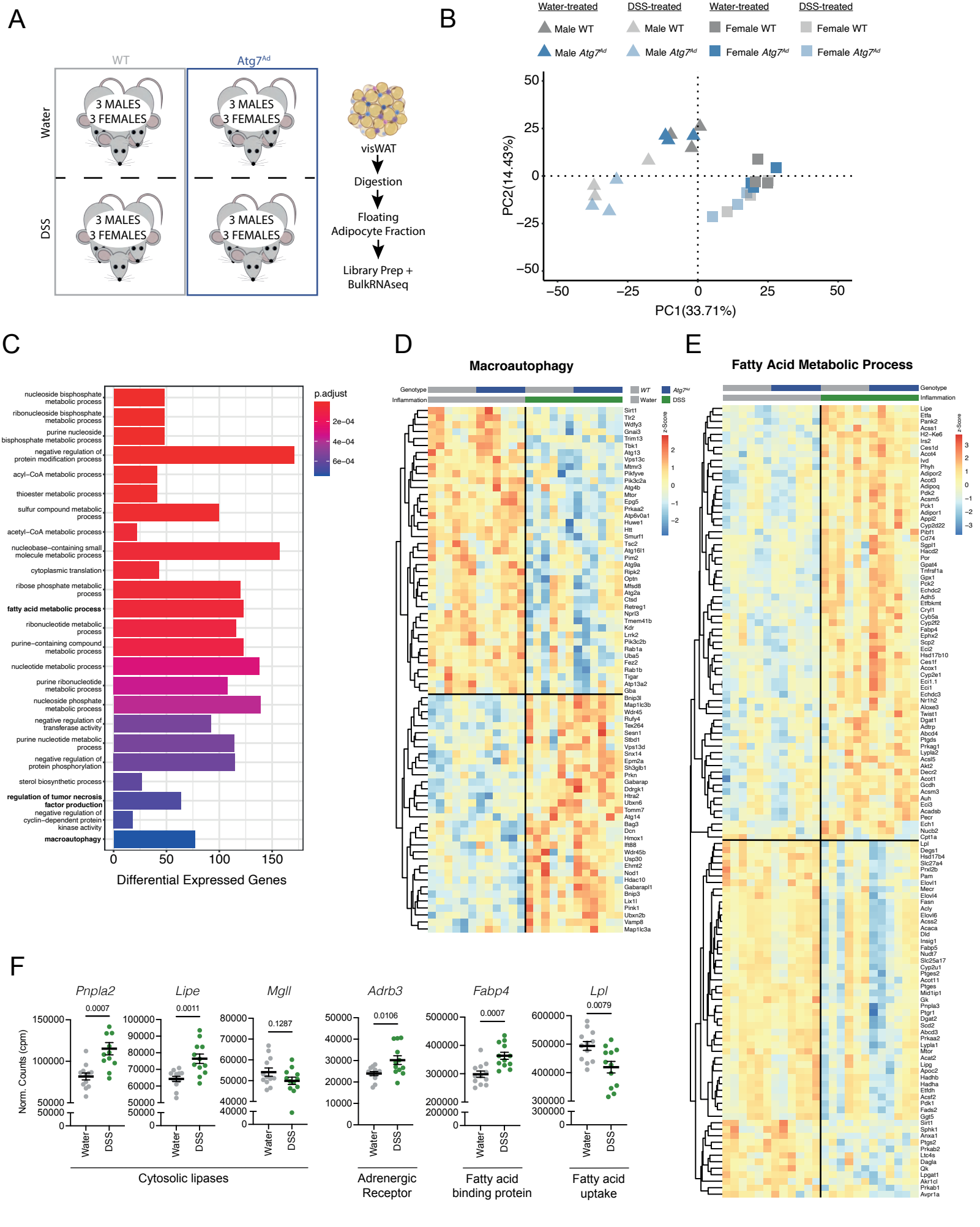
A
WT
Atg7Ad
Water
DSS
3 MALES
3 FEMALES
visWAT
Digestion
Floating
Adipocyte Fraction
Library Prep +
BulkRNAseq
B
Water-treated
DSS-treated
Water-treated
DSS-treated
Male WT
Male WT
Female WT
Female WT
Male Atg7Ad
Male Atg7Ad
Female Atg7Ad
Female Atg7Ad
PC2(14.43%)
PC1(33.71%)
C
p.adjust
2e−04
4e−04
6e−04
nucleoside bisphosphate metabolic process
ribonucleoside bisphosphate metabolic process
purine nucleoside bisphosphate metabolic process
negative regulation of protein modification process
acyl−CoA metabolic process
thioester metabolic process
sulfur compound metabolic process
acetyl−CoA metabolic process
nucleobase−containing small molecule metabolic process
cytoplasmic translation
ribose phosphate metabolic process
fatty acid metabolic process
ribonucleotide metabolic process
purine−containing compound metabolic process
nucleotide metabolic process
purine ribonucleotide metabolic process
nucleoside phosphate metabolic process
negative regulation of transferase activity
purine nucleotide metabolic process
negative regulation of protein phosphorylation
sterol biosynthetic process
regulation of tumor necrosis factor production
negative regulation of cyclin−dependent protein kinase activity
macroautophagy
Differential Expressed Genes
D
Macroautophagy
Genotype
Inflammation
WT
Atg7Ad
Water
DSS
z-Score
E
Fatty Acid Metabolic Process
Genotype
Inflammation
z-Score
F
Pnpla2
Lipe
Mgll
Adrb3
Fabp4
Lpl
0.0007
0.0011
0.1287
0.0106
0.0007
0.0079
Norm. Counts (cpm)
Water
DSS
Cytosolic lipases
Adrenergic Receptor
Fatty acid binding protein
Fatty acid uptake

Figure 5

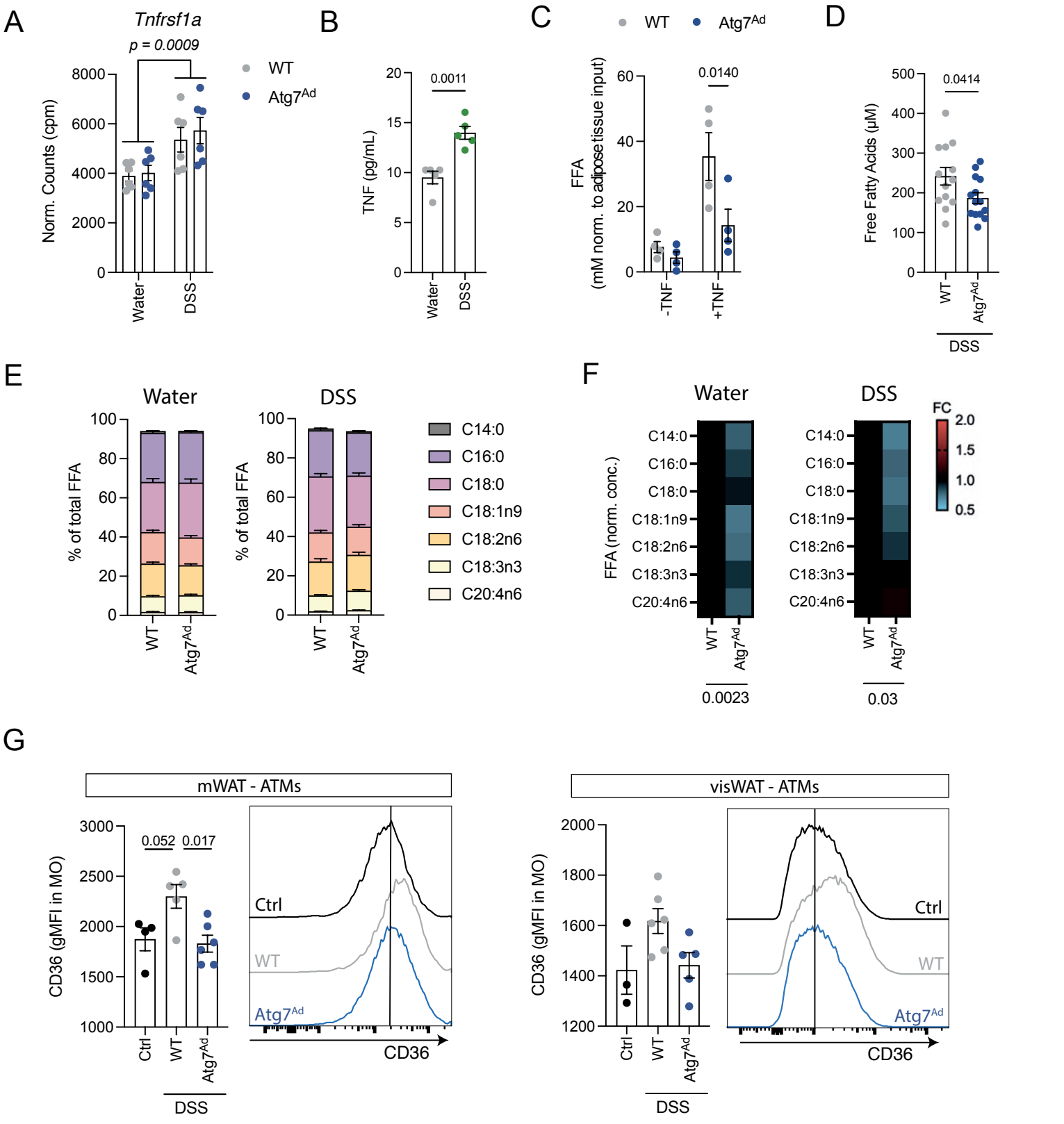
A
Tnfrsf1a
p = 0.0009
Norm. Counts (cpm)
WT
Atg7Ad
Water
DSS
B
TNF (pg/mL)
0.0011
C
FFA
(mM norm. to adipose tissue input)
0.0140
-TNF
+TNF
D
Free Fatty Acids (µM)
0.0414
E
Water
DSS
% of total FFA
C14:0
C16:0
C18:0
C18:1n9
C18:2n6
C18:3n3
C20:4n6
F
FFA (norm. conc.)
FC
2.0
1.5
1.0
0.5
0.0023
0.03
G
mWAT - ATMs
visWAT - ATMs
CD36 (gMFI in MO)
0.052
0.017
Ctrl
CD36

Figure 6

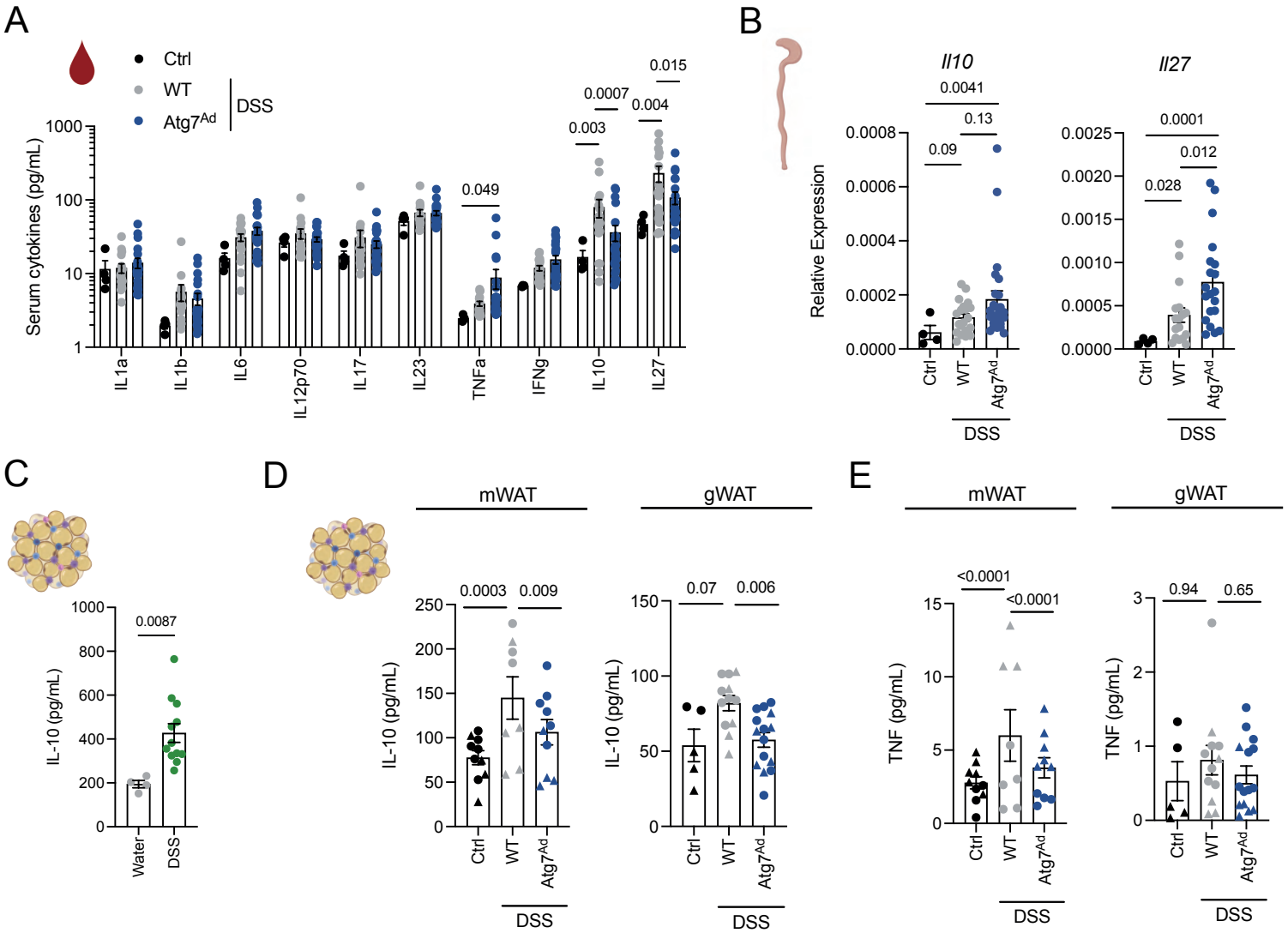
A
Ctrl
WT
Atg7Ad
DSS
Serum cytokines (pg/mL)
1000
100
10
1
0.049
0.003
0.0007
0.004
0.015
IL1a
IL1b
IL6
IL12p70
IL17
IL23
TNFa
IFNg
IL10
IL27
B
Il10
Il27
Relative Expression
0.0041
0.13
0.09
0.0001
0.012
0.028
0.0008
0.0006
0.0004
0.0002
0.0000
0.0025
0.0020
0.0015
0.0010
0.0005
Ctrl
WT
Atg7Ad
DSS
C
IL-10 (pg/mL)
0.0087
1000
800
600
400
200
0
Water
DSS
D
mWAT
gWAT
0.0003
0.009
0.07
0.006
250
200
150
100
50
0
150
100
50
0
Ctrl
WT
Atg7Ad
DSS
E
mWAT
gWAT
TNF (pg/mL)
<0.0001
<0.0001
0.94
0.65
15
10
5
0
3
2
1
0
Ctrl
WT
Atg7Ad
DSS

Figure 7

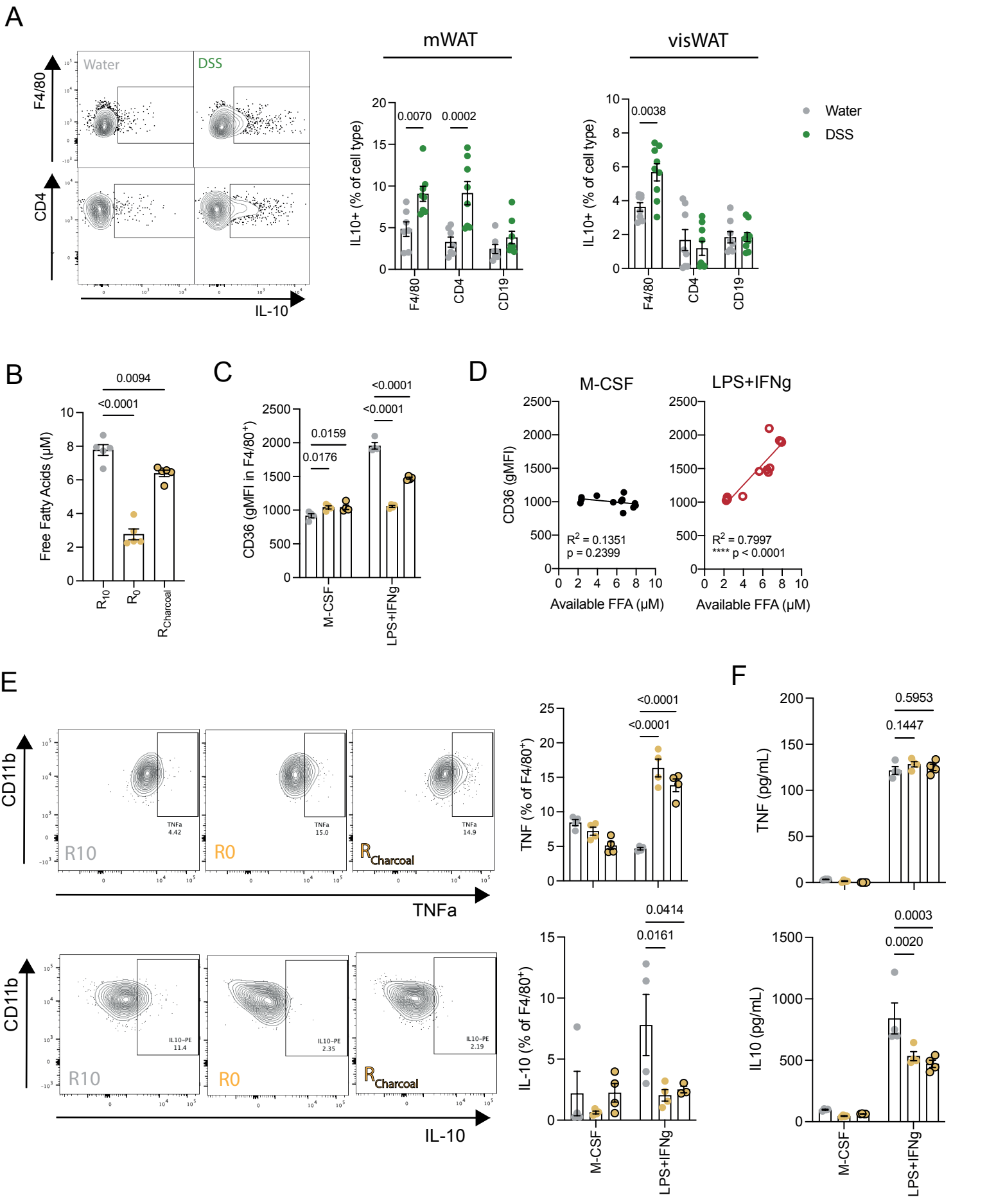
A
Water
DSS
F4/80
CD4
IL-10
mWAT
visWAT
IL10+ (% of cell type)
0.0070
0.0002
0.0038
F4/80
CD4
CD19
Water
DSS
B
0.0094
<0.0001
Free Fatty Acids (μM)
R10
R0
RCharcoal
C
<0.0001
<0.0001
0.0159
0.0176
CD36 (gMFI in F4/80+)
M-CSF
LPS+IFNg
D
M-CSF
LPS+IFNg
CD36 (gMFI)
R2 = 0.1351
p = 0.2399
R2 = 0.7997
**** p < 0.0001
Available FFA (μM)
E
CD11b
TNFa
IL-10
R10
R0
RCharcoal
TNFa 4.42
TNFa 15.0
TNFa 14.9
IL10-PE 11.4
IL10-PE 2.35
IL10-PE 2.19
TNF (% of F4/80+)
IL-10 (% of F4/80+)
<0.0001
<0.0001
0.0414
0.0161
F
TNF (pg/mL)
IL10 (pg/mL)
0.5953
0.1447
0.0003
0.0020
M-CSF
LPS+IFNg

Graphical Abstract